

Northumbria Research Link

Citation: Daramola, Alex S., Ahmadi, Seyed Ehsan, Marzband, Mousa and Ikpehai, Augustine (2023) A cost-effective and ecological stochastic optimization for integration of distributed energy resources in energy networks considering vehicle-to-grid and combined heat and power technologies. *Journal of Energy Storage*, 57. p. 106203. ISSN 2352-152X

Published by: Elsevier

URL: <https://doi.org/10.1016/j.est.2022.106203>
<<https://doi.org/10.1016/j.est.2022.106203>>

This version was downloaded from Northumbria Research Link:
<https://nrl.northumbria.ac.uk/id/eprint/51061/>

Northumbria University has developed Northumbria Research Link (NRL) to enable users to access the University's research output. Copyright © and moral rights for items on NRL are retained by the individual author(s) and/or other copyright owners. Single copies of full items can be reproduced, displayed or performed, and given to third parties in any format or medium for personal research or study, educational, or not-for-profit purposes without prior permission or charge, provided the authors, title and full bibliographic details are given, as well as a hyperlink and/or URL to the original metadata page. The content must not be changed in any way. Full items must not be sold commercially in any format or medium without formal permission of the copyright holder. The full policy is available online: <http://nrl.northumbria.ac.uk/policies.html>

This document may differ from the final, published version of the research and has been made available online in accordance with publisher policies. To read and/or cite from the published version of the research, please visit the publisher's website (a subscription may be required.)

1 A Cost-Effective and Ecological Stochastic Optimization
2 for Integration of Distributed Energy Resources in Energy
3 Networks Considering Vehicle-to-Grid and Combined
4 Heat and Power Technologies

5 Alex S. Daramola^a, Seyed Ehsan Ahmadi^a, Mousa Marzband^{a,b}, Augustine Ikpehai^c

6 ^aNorthumbria University, Electrical Power and Control Systems Research Group, Ellison Place NE1 8ST,
7 Newcastle upon Tyne, UK

8 ^bCenter of Research Excellence in Renewable Energy and Power Systems, King Abdulaziz University,
9 Jeddah, 21589, Saudi Arabia

10 ^cDepartment of Engineering and Mathematics, Sheffield Hallam University, Sheffield S1 1WB, UK

11 **Abstract**

Electric vehicles (EVs) have the potential to decarbonize the transport sector and contribute to the attainment of the global Net-Zero goal. However, to achieve sustainable decarbonization, EVs' power for grid-to-vehicle (G2V) operations should be sourced from carbon-free or low carbon power generating sources. Whilst the adoption of renewable energy sources (RES) in EVs' G2V process has been extensively explored, combined heat and power (CHP) technologies are underexamined. Hence, this paper deploys harmonized natural gas and fuel cell CHP technologies alongside RES and battery energy storage systems (BESS) to facilitate EVs' G2V and vehicle-to-grid (V2G) operations. While the BESS supports V2G operations and stores excess power from the CHP and RES, the CHP's by-product heat could be employed in heating homes and industrial facilities. Furthermore, to maximize environmental and economic benefits, the CHP technologies are designed following the hybrid electric-thermal load strategy, such that the system autonomously switches between following the electric load strategy and following the thermal load strategy. The proposed optimization problem is tested using three different case studies (CSs) to minimize the microgrid's (MG) operating costs and carbon dioxide (CO₂) emissions in a stochastic framework considering the RES generations, the load consumption, and the behavior patterns of charging/discharging periods of EVs as the

uncertain parameters. The first CS tests the proposed algorithm using only CHP technologies. Secondly, the algorithm is examined using the CHP technologies and RES. Finally, the BESS is added to support and analyze the impacts of the V2G operations of EVs on the MG. Furthermore, the life cycle assessment is investigated to analyse the CO₂ emissions of distributed generations. The results show a 32.22%, 44.49%, and 47.20% operating cost reduction in the first, second, and third CSs. At the same time, the CO₂ emissions declined by 29.13%, 47.13% and 47.90% in the various corresponding CSs. These results demonstrate the economic and environmental benefits of applying CHP with RES in facilitating G2V and V2G operations towards achieving a decarbonized transport sector.

¹² *Keywords:* Distributed Generation, Microgrid, CO₂ emission, Vehicle-to-Grid,
¹³ Combined Heat and Power, Fuel Cell.

¹⁴ **Nomenclature**

Acronyms

	EV	Electric Vehicle
	CHP	Combined heat and power
	BESS	Battery energy storage system
	CO ₂	Carbon dioxide
	V2G	Vehicle-to-grid
	G2V	Grid-to-vehicle
¹⁵	GHG	Greenhouse gases
	RES	Renewable energy sources
	MG	Microgrid
	PV	Photovoltaic
	WT	Wind turbine
	DG	Distributed generation
	SBA	Scenario-Based Analysis
	SoC	State of charge

PGU	Power generation unit
FELD	Following electrical load demand
FTLD	Following thermal load demand

Indices

K_{PGU}	Constant index of the PGU
K_{FCU}	Constant index of the fuel cell unit
K_{CHP}	Constant index of the CHP
γ_{NG}	Emission conversion factor of the natural gas
γ_{GRID}	Emission conversion factor of the grid

Parameters

η_{HRU}	Efficiency of the heat recovery unit [%]
η_{PGU}	Efficiency of the PGU [%]
η_{FR}	Efficiency of the fuel reformer [%]
η_{FCU}	Efficiency of the fuel cell unit [%]
η_{BOILER}	Boiler's thermal efficiency [%]
¹⁶ η^{EV+}, η^{EV-}	Charging/Discharging Efficiency of the EV [%]
$T_{Ch}^{Day}, T_{Dch}^{Day}$	Charging/ Discharging period of EV [Hours]
$SOC^{EV, Dep}$	State of charge of EV battery in departure time [%]
λ^{CO_2}	Price of CO ₂ emission [£/kg CO ₂]
μ_s	Probability of scenario s [0-1]

Decision variables

H_{FR}	Hydrogen from the fuel reformer [kg]
N_{FR}	Natural gas consumed by the fuel reformer [MMBTU/hour]
E_{PGU}	Total electricity derived from the [MWh]
N_{PGU}	Natural gas consumed by the PGU [MMBTU/hour]
E_{FCU}	Electricity generated by the fuel cell unit [MWh]
H_{FCU}	Hydrogen consumption of the fuel cell unit [kg]
Q_{PGU}, Q_{FR}	Heat recovered from the PGU/ fuel reformer [MMBTU/hour]
Q_{HRU}	Recovered heat passing through the heat recovery unit [MMBTU/day]
E_{total}^{CHP}	Total electricity produced by the CHP [MWh]
E_{req}	Electricity required by the EVs and buildings [MWh]

$Q_{\text{req}}^{\text{building}}$	Heat required to meet the building's heat load [MMBTU/hour]
Q_{BOILER}	Heat supplied by auxiliary boiler [MMBTU/hour]
E_{GRID}	Additional electricity purchased from the grid [MWh]
N_{TOTAL}	Total natural gas consumed by the PGU and fuel reformer [MMBTU]
N_{BOILER}	Natural gas consumed by the boiler [MMBTU/hour]
$\text{Cost}_{\text{CHP-FHL}}$	Cost of operating the CHP [GBP]
CD_{Emission}	Total CO ₂ emission in the system [kg CO ₂ /MWh]
$\text{SOC}_t^{\text{EV}}, \text{SOC}_t^{\text{BESS}}$	State of charge of EV/ BESS at time t [Hours]
$\underline{\text{SOC}}_t^{\text{BESS}}, \overline{\text{SOC}}_t^{\text{BESS}}$	Minimum/ Maximum state of charge of BESS [%]
$\underline{\text{SOC}}_t^{\text{EV}}, \overline{\text{SOC}}_t^{\text{EV}}$	Minimum/ Maximum state of charge of EV [%]
$P_{\text{Total}}^{\text{EV}}$	Total energy that can be stored in the EV [MWh]
$P_t^{\text{EV+}}, P_t^{\text{EV-}}$	Charging/ Discharging power of the EV at time t [MW]
$P_t^{\text{PV}}, P_t^{\text{WT}}, P_t^{\text{CHP}}$	Power produced by the PV/ WT/ CHP at time t [MW]
$P_t^{\text{BESS-}}, P_t^{\text{BESS+}}$	Power supplied/ required by/ to charge the BESS at time t [MW]
$P_t^{\text{grid-}}, P_t^{\text{grid+}}$	Power purchased/ sold from/ to the grid at time t [MW]
$\overline{P}_t^{\text{BESS+}}, \overline{P}_t^{\text{BESS-}}$	Maximum power required/ discharged to charge/ by the BESS [MW]

18 1. Introduction

19 1.1. Motivation

20 Environmental sustainability is growing into a household discussion due to re-
21 cent large-scale climate disasters such as the Attica wildfires in Greece, flooding
22 in Australia, extensive wildlife migration and the unfavourable prevailing weather
23 conditions. Although it cannot be ascertained with certainty how much average
24 global temperature will increase, the significant impacts of global warming have
25 been seen, and failing to take actions to prevent the consequences of further warm-
26 ing may show floundering [1]. To this end, climate change discussions have been at
27 the forefront of governmental panels and meetings. The 2021 United Nations Cli-
28 mate Change Conference, commonly termed COP26, was explicitly set up to bring
29 different global players and world leaders to discuss and agree on ways to miti-
30 gate greenhouse gas (GHG) emissions and keep the average global temperature of

31 1.5°C within reach. Therefore, expediting the removal of fossil fuel-fired power
32 plants and facilitating the switch to electric vehicles (EV) are proposed as some
33 of the ways to secure global Net-Zero by 2050 [2]. However, the large-scale de-
34 ployment of EVs leads to extensive network reinforcements, unbalanced voltage,
35 increased load demand, raised operating costs and high electrical strain on the ex-
36 isting power distribution network. This paper explores a decentralized approach
37 to alleviate some of these challenges and lower carbon dioxide (CO₂) emissions
38 by investigating the integration of co-generation plants such as combined heat and
39 power (CHP) and renewable energy technologies into the distribution network to
40 support expansive EV use.

41 Currently, internal combustion engine (ICE) vehicles make up around 10% of
42 universal carbon dioxide emissions, and oil-derived fuels account for roughly 95%
43 of the energy expended in the transportation sector [3, 4]. Conversely, CHP tech-
44 nologies can lower CO₂ emissions by around 32% compared to the conventional
45 way of separately generating electricity and heat [5]. Hence, the mass deployment
46 of EVs alongside grid incorporated CHP and renewable energy sources (RES) can
47 decarbonize the power distribution network and contribute to the electrification of
48 the transport sector. However, EVs currently constitute a small but rapidly expand-
49 ing part of the transport market. Notwithstanding, EVs are promising substitutes
50 for fossil fuel drivetrains as they offer more carbon benefits than ICEs. They do not
51 produce tank-to-wheel GHGs and have higher tank-to-wheel efficiency than other
52 drivetrains. In addition, EVs can shape power demand curves during on-peak or off-
53 peak periods. [6, 7] discussed the optimal deployment of grid-to-vehicle (G2V) and
54 vehicle-to-grid (V2G) infrastructures in reconciling the differential gap in power
55 supply and demand, minimizing charging, and discharging costs, reducing GHG
56 emissions and maximizing the profits of EV owners. Furthermore, the incorpora-
57 tion of small-scale distributed CHP technologies, photovoltaic (PV) systems, wind
58 turbines (WT), fuel cells and battery energy storage systems (BESS) into the exist-
59 ing power distribution network offers the advantages of achieving lower operating
60 costs, reduced CO₂ emissions and network reinforcement in aiding the flexible G2V
61 and V2G operations of EV [8].

62 Moreover, an essential factor to evolve toward a cleaner and cost-effective en-
63 ergy system is to develop multi-energy system (MES). A MES can feature better
64 technical, economic and environmental performance relative to independent en-
65 ergy systems. A MES has multiple terminal resources and multiple distributed com-
66 ponents for energy generation, conversion, and storage. Therefore, a networked
67 energy system with optimized multi-energy resources can be designed [9]. By tak-
68 ing into account the MES districts, recent studies have indicated that distributed
69 generation (DG) can provide major advantages by integrating complementary tech-
70 nologies such as harmonized natural gas and fuel cell CHP units. In fact, they can
71 locally generate electricity and heat, while significantly decreasing operating costs,
72 thus offering enhanced flexibility in supplying the electricity grid [10, 11]. Hence,
73 this paper aims to achieve these stated merits using a decentralized novel approach
74 that will support EVs' mass use and contribute to decarbonizing the transport sector
75 in a MES framework.

76 1.2. Literature review

77 Many studies have been conducted on the design and operation of CHP systems.
78 Most of these studies have focused on establishing an integrated system among di-
79 verse energy sectors. Authors in [12–15] have designed the CHP system on the
80 basis of proton exchange membrane fuel cells (PEMFC) integrated with methanol-
81 reforming and dehumidification to supply electricity/thermal demand, enhance the
82 utilization of RES, and reduce the energy consumption and environmental pollu-
83 tion. Also, the effects of operating parameters of PEMFC and refrigeration system
84 on the energy, exergy, economy and environment are studied over a multi-objective
85 optimization approach. Furthermore, the ongoing energy transition has led to
86 diverse research in the electrification of road transport to address its impact on the
87 environment and achieve the global Net-Zero targets. According to [16–18], EVs
88 will play a principal role in attaining the Net-Zero targets due to their higher en-
89 ergy efficiency and ability to use energy from RESs for G2V operations. Also, when
90 connected to the power distribution network, EVs could support the grid (V2G oper-
91 ations), balance supply and demand, and thus, facilitate the incorporation of RESs.

92 Nevertheless, the authors in [16–18] did not give much attention to reducing CO₂
93 emissions. Also, the authors did not consider strategies of lowering the operating
94 costs and analysing the uncertainties.

95 The cost-optimization method suggested by [19–21] uses the optimal scheduling
96 of EV charging as a means to lower the overall cost of the system, reduce network
97 losses and enhance power quality. These optimization approaches explored the use
98 of global and local optimization methods, smart meters and optimal placement of
99 the charging points at different sections of the power network. However, while
100 these studies offered some operating costs reduction, they failed to consider the
101 environmental implications of the widespread of EVs on the existing electricity grid
102 and deploy small scale carbon-free or low carbon distributed generation sources
103 to support the existing grid and minimize GHG emissions. A more comprehensive
104 approach, such as that seen in the [22] study, implemented a multi-objective techno-
105 economic environmental optimization model to concurrently reduce the electricity
106 running cost, carbon dioxide emissions, grid utilization and EVs' battery degrada-
107 tion. Although the authors extensively highlighted the economic and environmental
108 benefits of EVs' deployment in [19–22], they did not take into account the integra-
109 tion of highly efficient CHP technologies and multi-RES in reinforcing the power
110 distribution network. Also, they did not consider the uncertainty of the renewable
111 generations and load consumption.

112 Authors in [23] have investigated the optimal sizing of a hybrid PV-battery-diesel
113 system in curtailing the overall costs of EVs in a V2G enabled parking lot. The au-
114 thors applied a heuristic optimization approach in deciding the optimal size of the
115 hybrid system, which led to a 5.21% reduction in the system's overall cost. But the
116 CO₂ benefit of this system was not analyzed, and the achieved cost minimization
117 is a bit low when compared with other related studies. [24] explored the addi-
118 tion of hybrid solar-wind energy sources with the distribution network to reduce
119 the computational cost of the optimal power flow calculations in EV charging op-
120 erations. The authors employed a parallel epsilon variable multi-objective genetic
121 algorithm to solve the probabilistic optimal power flow, and the results obtained
122 validated the effectiveness of the proposed method. Furthermore, a concession of

123 30.13% and 16.94% in load peak-to-valley and standard deviation were achieved
124 by [25] research exploring the orderly scheduling of EV charging using deep learn-
125 ing. The authors combined the convolutional neural network and deep belief net-
126 work, which they termed CNN-DBN, to predict the load demand and outputs of the
127 RESs required to charge the EVs while lowering the distribution network's operat-
128 ing costs. In this framework, the network's economic aspect is considered, while the
129 integration of BESS and distributed CHP technologies to reduce CO₂ emissions and
130 operational costs were not examined. Similarly, [26] proposed an integrated Grey
131 Wolf Optimizer and Taguchi test method as a promising approach for minimizing
132 microgrid procurement costs, reducing power losses and CO₂ emissions of the dis-
133 tribution network to aid the extensive use of EVs. The writers tested the adequacy
134 of this method on a modified IEEE 69-bus system to justify the recommended ap-
135 proach. Although the uncertain parameter are considered in the operation problem,
136 research pieces in [23–26] failed to employ a BESS to support the V2G operations
137 in meeting power demand at peak demand periods. Furthermore, [27] investigated
138 the co-location of CHP units for the fast charging of EVs, which is crucial in encour-
139 aging the mass use of EVs, as it addresses the concern on EV prolong charging. The
140 authors analyzed three different CHP configurations to find the most fuel-efficient
141 strategy, explored the charging behaviour of EV drivers and showcased the advan-
142 tage of variable speed generators over fixed speed counterpart in lowering the CHP's
143 fuel consumption. However, they failed to inspect the CO₂ impact of the CHP unit
144 or consider a fuel cell CHP strategy to curb the system's environmental footprints.
145 Besides, they did not take into account the uncertainties of the system.

146 Table 1 provides a summarised view of the previous papers within the research
147 focus and their various limitations. [Some research gaps \(RG\) recognized in the](#)
148 [reviewed literature can be mentioned as follows:](#)

149 **RG1:** [The economic and environmental analysis of V2G facility and CHP technol-](#)
150 [ogy in supporting the existing power distribution network, lowering CO₂](#)
151 [emissions, and minimizing the operating costs were not explicitly proposed](#)
152 [in a stochastic framework.](#)

Table 1: A comparative summary of previous papers and this research

Ref.	Uncertain Parameters			Objective Function		Operation Units				
	Load	RES	EV	CO ₂ Emission	Operating Cost	CHP Unit	Fuel Cell	RES	BESS	V2G
[16]	✗	✗	✗	✓	✗	✗	✗	✓	✗	✗
[17]	✗	✗	✗	✓	✗	✗	✗	✓	✗	✗
[18]	✗	✗	✗	✓	✗	✗	✗	✓	✗	✗
[19]	✗	✗	✗	✓	✓	✗	✗	✗	✗	✓
[20]	✗	✗	✓	✓	✓	✗	✗	✗	✗	✓
[21]	✗	✗	✗	✓	✓	✗	✗	✗	✗	✗
[22]	✗	✗	✗	✓	✓	✗	✗	✓	✗	✓
[23]	✗	✓	✗	✓	✓	✗	✗	✓	✓	✓
[24]	✓	✓	✓	✓	✓	✗	✗	✓	✗	✗
[25]	✓	✓	✓	✓	✓	✗	✗	✓	✗	✗
[26]	✗	✓	✗	✓	✓	✓	✗	✓	✗	✓
[27]	✗	✗	✗	✓	✓	✓	✗	✓	✗	✗
This Paper	✓	✓	✓	✓	✓	✓	✓	✓	✓	✓

153 **RG2:** The integration of BESS and RESs to support V2G facility and CHP technology
 154 during peak load hours and minimize the wastage of excess power from the
 155 CHP units are not taken into account in the reviewed papers.

156 **RG3:** Previous works did not take any additional measures to lower the carbon
 157 footprints of the grid integrated CHP technologies to decarbonize its opera-
 158 tions and minimize the overall CO₂ emission of the system.

159 1.3. Research contributions

160 The electricity and transport sectors are getting increasingly connected. Hence,
 161 most of the energy for charging EVs will come from the national electricity grid,
 162 which is currently dominated by high operational expenses and large fossil fuel-
 163 driven power plants. Therefore, this paper focuses on minimizing the power distri-
 164 bution network's operating and CO₂ emissions costs in aiding the mass deployment
 165 of EVs. It examines the integration of harmonized natural gas and fuel cell CHP
 166 technologies, PVs arrays, WTs, and BESS in a stochastic energy management of the
 167 existing power distribution network. Furthermore, it investigates the benefits of

168 operating V2G and G2V strategies in the power network. For the sake of a detailed
169 analysis of the CO₂ emissions, the life cycle assessment (LCA) is also calculated.

170 Based on the mentioned RGs in the reviewed pieces of literature, the following
171 research contributions (RC) are made:

172 **RC1:** Employ an hourly cost-effective-based G2V and V2G strategies to support the
173 electricity grid network, facilitate peak shaving in high power demand peri-
174 ods, and act as an on-demand carbon-free energy source (Addresses **RG1**).

175 **RC2:** Investigate the economic and environmental contributions of BESS in aiding
176 V2G and G2V facilities, reducing wastage of excess power, minimizing CO₂
177 emissions, and lowering the overall operating costs of power network and EV
178 owners (Addresses **RG2**).

179 **RC3:** Model and formulate a harmonized natural gas and fuel cell CHP system
180 following the hybrid electric-thermal strategy. Besides, integrate a natural
181 gas fuel reformer with the CHP technology to provide the hydrogen required
182 to operate the fuel cell units in the harmonized CHP system, thus, reducing
183 the carbon footprints of the CHP output. (Addresses **RG3**).

184 2. Model and problem formulation

185 2.1. Life Cycle Assessment

186 LCA includes four stages, goal and scope definition, life cycle inventory analysis,
187 life cycle impact assessment and interpretation. These stages are summarized in
188 Figure 1 for a proper illustration [28].

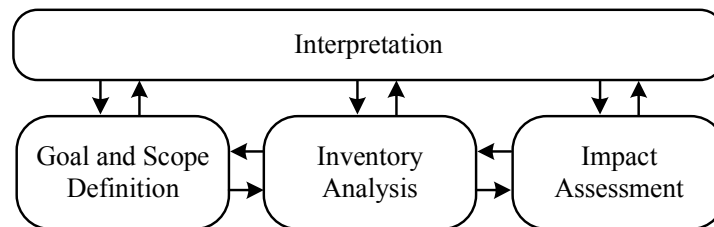


Figure 1: Life cycle assessment framework.

189 To explain briefly each stage; goal and scope definition enables the system oper-
 190 ator to determine the goal of the proposed research, to set physical and dimensional
 191 system limitations, and to determine which type of LCA to utilize. The inventory
 192 analysis is commonly the most work intensive stage and contains collecting of life
 193 cycle inventory data for all foundations modelled processes and integration of those
 194 data into the greater model. Impact assessment implies calculation of emissions and
 195 impacts. In the interpretation stage, the system operator analyses the outcomes of
 196 the impact assessment, and may select from a variety of interpretation implements
 197 to support this analysis. There is continual feedback among the diverse stages, as
 198 shown by the arrows in Figure 1, as data disclosed in various stages affects decisions
 199 and outcomes in preceding and subsequent stages [29].

200 Environmental life cycle impact categories associate to atmospheric, aquatic and
 201 terrestrial impacts due to material release or exhaustion in the environment. The
 202 global warming potential is the major recognized environmental impact category
 203 influencing the net zero GHG strategies. In this paper, the mathematical equations
 204 and approaches for environmental LCA of DERs including PV, WT, and CHP unit are
 205 defined. For the brevity of the LCA model of this paper, its scope has been confined
 206 to the analysis at the global warming potential (amount of CO₂eq). The environ-
 207 mental life cycle impact characterization of a material in an impact category is the
 208 alteration in its fundamental property responsible for the category due to alteration
 209 in its plenty in the environment with respect to the alteration of a reference material
 210 as demonstrated in Eq. (1).

211

$$\text{LCIA}_{j=y,k} = \frac{\int_0^{\text{TH}} \alpha_{j=y,k} y(t) dt}{\int_0^{\text{TH}} \alpha_{j=y,k} r(t) dt} \quad (1)$$

212

213 $\text{LCIA}_{j=y,k}$ is the life cycle impact characterization of a material y in an impact
 214 category k . $\alpha_{j,k}$ is the fundamental property increase of the material y or relative
 215 material r for its unit application alternation in the environment. The function of
 216 time $y(t)$ is the alternation in plenty due to prompt release or exhaustion of the
 217 material. TH is the period of the computation. As the life cycle impact character-
 218 ization of a material in an impact category is the ratio with respect to a reference

219 material, the unit of life cycle impact characterization of a material is mass of the
 220 reference material equal. An absolute environmental impact in a category E_k can
 221 be calculated applying Eq. (2).
 222

$$E_k = \sum_j LCIA_{j,k} \times m_j \quad (2)$$

223 where, m_j is the quantity or inventory of the pollutant j emitted to the environ-
 224 ment [30].
 225

226 2.2. Scenario-based analysis for modelling uncertainty

227 As the RES generations, the load consumption, and the behavior patterns of
 228 charging/discharging periods of EVs are uncertain and stochastic, employing a de-
 229 terministic framework will not guarantee a thorough insight into the potential ben-
 230 efits of integrating distributed energy resources [31]. To properly handle the un-
 231 certainties, a scenario-based analysis (SBA) is used to generate the number of sce-
 232 narios as well as a backward scenario reduction strategy to decrease them. More
 233 details on the scenario reduction strategy can be found in [32]. In SBA method,
 234 the Probability Density Function (PDF) curve of the uncertain parameter is divided
 235 into multiple levels. Applying the PDF, the probability of the uncertain variable in
 236 each level can be calculated. Stochastic framework is modeled in this paper as a
 237 normal Gaussian PDF, where the mean is equal to the forecasted value. In major
 238 samples, the forecasted value is considered as the standard deviation of PDF. The
 239 formulation of the normal Gaussian PDF is presented as Eqs. (3).
 240

$$f(x|m, \vartheta^2) = \frac{1}{\sqrt{2\pi\vartheta^2}} \exp\left(-\frac{(x-m)^2}{2\vartheta^2}\right), \quad -\infty < x < +\infty \quad (3)$$

241 where x indicates the uncertain parameter, m is the mean of the forecasted input
 242 variable, ϑ^2 is the variance and ϑ is the standard deviation of the forecasted input
 243 variable. Figure 2 demonstrates the normal PDF divided into multiple segments
 244 with diverse probability levels [33].
 245

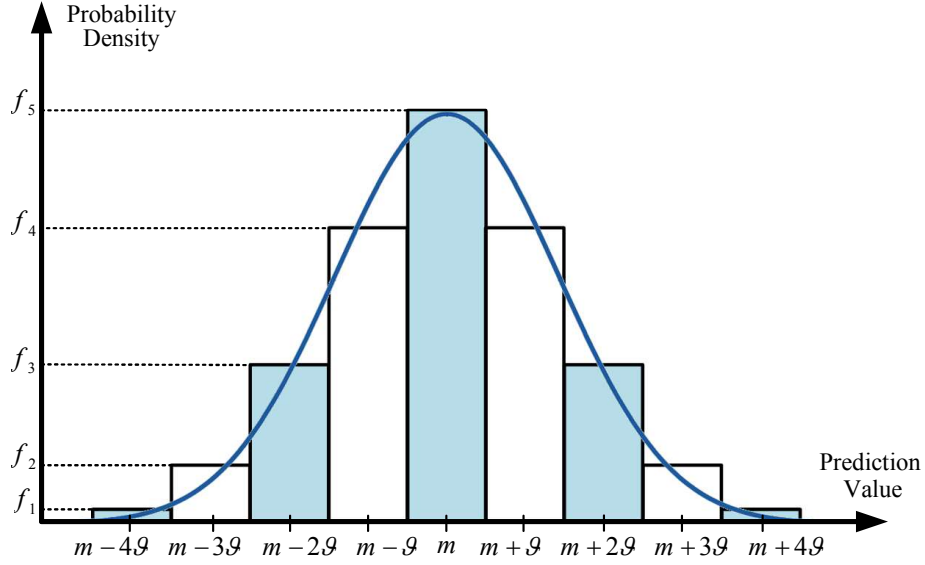


Figure 2: Normal probability distribution function related to the standard deviation of prediction.

246 2.3. Modelling a harmonized natural gas and fuel cell CHP system

247 Figure 3 presents the single line diagram of the harmonized natural gas and hy-
 248 drogen fuel cell CHP technologies, which are modelled following the hybrid electric-
 249 thermal strategy. The mathematical models are a function of the amount of natural
 250 gas supplied to the power generation unit (PGU) and the fuel reformer. Hence, the
 251 efficiency of the PGU is expressed as Eq. (4).

252

$$\eta_{\text{PGU}} = \frac{E_{\text{PGU}}}{N_{\text{PGU}}} \quad (4)$$

253 where E_{PGU} is the total electricity (kWh) derived from the power generation unit,
 254 and N_{PGU} is the natural gas consumed by the PGU. Also, the efficiency of the PGU
 255 is assumed constant and is independent of the electric load demand.

256 Similarly, the efficiency of the fuel reformer and fuel cell unit are determined
 257 Eqs. (5) and (6), respectively.

259

$$\eta_{\text{FR}} = \frac{H_{\text{FR}}}{N_{\text{FR}}} \quad (5)$$

$$\eta_{\text{FCU}} = \frac{E_{\text{FCU}}}{H_{\text{FCU}}} \quad (6)$$

260 where H_{FR} and N_{FR} are the hydrogen from the fuel reformer and natural gas con-
 261 sumed by the fuel reformer, respectively. E_{FCU} is the electricity generated by the
 262 fuel cell unit and H_{FCU} is the hydrogen consumption of the unit.

263 In addition, the fuel reformer and fuel cell unit efficiencies are constant and
 264 are independent of the heat load and electric load, respectively. Therefore, the
 265 hydrogen from the fuel reformer is equal to the hydrogen inputted into the fuel cell
 266 unit. Hence, Eqs. (7) and (8) can be obtained from Eqs. (5) and (6) [34].

$$H_{FR} = \eta_{FR} \times N_{FR} = H_{FCU} \quad (7)$$

$$E_{FCU} = \eta_{FCU}(\eta_{FR} \times N_{FR}) \quad (8)$$

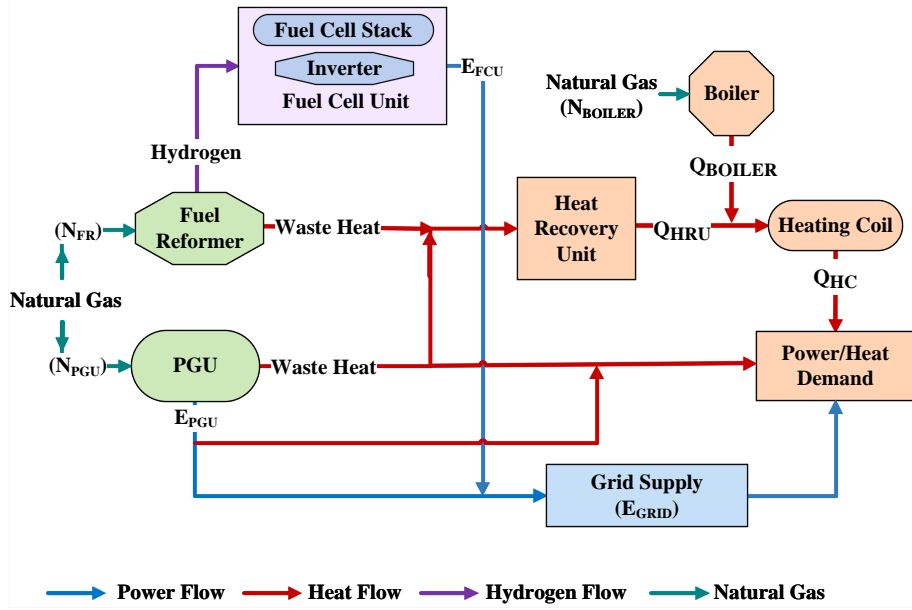


Figure 3: Schematic of a harmonized natural gas and fuel cell CHP system.

269 The by-product heat recovered from the PGU and passed through the heat re-
 270 covery unit can be estimated as the difference between the PGU natural gas con-
 271 sumption and the electricity produced by the PGU, multiplied by the efficiency of
 272 the heat recovery unit as demonstrated in Eq. (9) [34].

$$Q_{PGU} = (N_{PGU} - E_{PGU}) \times \eta_{HRU} \quad (9)$$

274 where Q_{PGU} is the recovered heat from the PGU and η_{HRU} is the efficiency of the
 275 heat recovery unit. By substituting Eq. (4) into Eq. (9), Eq. (10) is obtained.

$$Q_{PGU} = N_{PGU}(1 - \eta_{PGU}) \times \eta_{HRU} \quad (10)$$

277 Correspondingly, the heat recovered from the fuel reformer and into the heat
 278 recovery unit can be approximated as Eq. (11).

$$Q_{FR} = (N_{FR} - H_{FR}) \times \eta_{HRU} = (N_{FR} - \frac{E_{FCU}}{\eta_{FCU}}) \times \eta_{HRU} \quad (11)$$

280 Also, by substituting Eq. (8) into Eq. (11), Eq. (12) is obtained.

$$281 \quad Q_{FR} = [N_{FR} - \frac{\eta_{FCU}(\eta_{FR} \times N_{FR})}{\eta_{FCU}}] \times \eta_{HRU} = N_{FR}[1 - \frac{\eta_{FCU} \times \eta_{FR}}{\eta_{FCU}}] \times \eta_{HRU} \quad (12)$$

282 where Q_{FR} is the heat recovered from the fuel reformer. Thus, the amount of heat
 283 recovered from the power generation unit and the fuel reformer depends on the
 284 amount of natural gas they consume. The recovered heat passing through the heat
 285 recovery unit is then stated as as Eq. (13).

$$Q_{HRU} = Q_{PGU} + Q_{FR} \quad (13)$$

287 From Eq. (4) and Eq. (10), the electricity produced by the PGU can be written
 288 as as Eq. (14).

$$E_{PGU} = \frac{\eta_{PGU}}{(1 - \eta_{PGU}) \times \eta_{HRU}} Q_{PGU} \quad (14)$$

290 Also, using Eq. (8) and Eq. (12), the electricity produced by the fuel cell unit is
 291 expressed as as Eq. (15):

$$E_{FCU} = \frac{\eta_{FCU} \times \eta_{FR}}{(1 - \frac{\eta_{FCU} \times \eta_{FR}}{\eta_{FCU}}) \times \eta_{HRU}} Q_{FR} \quad (15)$$

293 Since the expressions multiplied by the variables Q_{PGU} and Q_{FR} comprise of
 294 only constant variables, they can be expressed as new constant K_{PGU} and K_{FCU} , as
 295 presented in Eqs. (16) and (17), respectively.

$$296 \quad K_{PGU} = \frac{\eta_{PGU}}{(1 - \eta_{PGU}) \times \eta_{HRU}} \quad (16)$$

$$297 \quad K_{FCU} = \frac{\eta_{FCU} \times \eta_{FR}}{(1 - \frac{\eta_{FCU} \times \eta_{FR}}{\eta_{FCU}}) \times \eta_{HRU}} \quad (17)$$

298 Thus, Eqs. (14) and (15) can be rewritten as Eqs. (18) and (19), respectively.

$$E_{PGU} = (K_{PGU})Q_{PGU} \quad (18)$$

300

$$E_{FCU} = (K_{FCU})Q_{FR} \quad (19)$$

301 From Eqs. (18) and (19), it is clear that the electricity generated by the CHP
 302 system is a linear function of the heat recovered. Hence, the total electricity pro-
 303 duced by the harmonized natural gas and fuel cell CHP system following the hybrid
 304 electric-thermal strategy is then determined as demonstrated in Eq. (20).

$$E_{total}^{CHP} = E_{PGU} + E_{FCU} = (K_{PGU})Q_{PGU} + (K_{FCU})Q_{FR} \quad (20)$$

306 Using the above linear equations, a perfect match between the electrical and
 307 thermal loads can be found [35]. However, due to the fluctuation in the energy re-
 308 quired by the electrical load (EVs and buildings) and the buildings' heat demands,
 309 it is difficult to continuously match both the electricity and heat demands. There-
 310 fore, to reduce the excess electricity or heat generated by the CHP, avoid wastage
 311 and minimize unwarranted CO₂ emissions, the CHP system operating in the hybrid
 312 electric-thermal load strategy is designed to autonomously follow the best optimal
 313 operations by switching between following electrical load demand (FELD) and fol-
 314 lowing thermal load demand (FTLD) strategies.

315 For $E_{req} < (K_{CHP})Q_{req}^{building}$, the FELD strategy will be followed for the CHP sys-
 316 tem. Also, for $E_{req} > (K_{CHP})Q_{req}^{building}$, the FTLD strategy will be selected. E_{req} is the
 317 electricity required by the EVs and buildings. Furthermore, (K_{CHP}) represents a
 318 constant coefficient. While $Q_{req}^{building}$ is the heat required to meet the building's heat
 319 load. Therefore, the electricity generated by the harmonized CHP system can be
 320 determined as Eqs. (21) and (22).

$$323 \quad \text{if } E_{req} < (K_{CHP})Q_{req}^{building}, \quad E_{total}^{CHP} = E_{req} \quad (21)$$

$$322 \quad \text{if } E_{req} > (K_{CHP})Q_{req}^{building}, \quad E_{total}^{CHP} = E' = (K_{CHP})Q_{req}^{building} \quad (22)$$

324 Using Eqs. (21) and (22), the heat captured by the heat recovery unit can be
 326 expressed as Eqs. (23) and (24).

$$327 \quad \text{if } E_{req} < (K_{CHP})Q_{req}^{building}, \quad Q_{HRU} = Q' = \frac{E_{total}^{CHP}}{K_{CHP}} \quad (23)$$

329

328

$$\text{if } E_{req} > (K_{CHP})Q_{req}^{building}, \quad Q_{HRU} = Q_{req}^{building} \quad (24)$$

330 When the CHP switches to the FELD strategy mode ($E_{\text{req}} < (K_{\text{CHP}})Q_{\text{req}}^{\text{building}}$), an
 332 auxiliary boiler (Q_{BOILER}) supplies the supplementary heat required by the buildings
 333 as in Eq. (25).

$$Q_{\text{BOILER}} = Q_{\text{req}}^{\text{building}} - Q' = Q_{\text{req}}^{\text{building}} - \frac{E_{\text{req}}}{K_{\text{CHP}}} \quad (25)$$

335 Also, when the CHP switches operation to the FTLD strategy mode ($E_{\text{req}} >$
 336 $(K_{\text{CHP}})Q_{\text{req}}^{\text{building}}$), the additional electricity required to power the buildings and EVs
 337 chargers is purchased from the electricity grid (with incorporated RESs) and defined
 338 as in Eq. (26).

$$E_{\text{GRID}} = E_{\text{req}} - E' = E_{\text{req}} - (K_{\text{CHP}})Q_{\text{req}}^{\text{building}} \quad (26)$$

340 The total amount of natural gas consumed by the power generation unit, fuel
 341 reformer (for hydrogen production) and the auxiliary boiler are denoted in Eqs. (27)
 342 and (28) for FELD and FTLD strategies, respectively.

$$\text{FELD: } N_{\text{total}} = N_{\text{PGU}} + N_{\text{FR}} + N_{\text{BOILER}} = \frac{E_{\text{PGU}}}{\eta_{\text{PGU}}} + \frac{E_{\text{FCU}}}{\eta_{\text{FCU}} \times \eta_{\text{FR}}} + \frac{Q_{\text{BOILER}}}{\eta_{\text{BOILER}}} \quad (27)$$

345
 344

$$\text{FTLD: } N_{\text{total}} = N_{\text{PGU}} + N_{\text{FR}} = \frac{E_{\text{PGU}}}{\eta_{\text{PGU}}} + \frac{E_{\text{FCU}}}{\eta_{\text{FCU}} \times \eta_{\text{FR}}} \quad (28)$$

346 where N_{BOILER} is natural gas consumed by the boiler, and η_{BOILER} is the boiler's
 348 thermal efficiency. The cost of operating the harmonized CHP system in the hybrid
 349 strategy mode is expressed as Eq. (29).

$$\text{cost}_{\text{CHP-FHL}} = (N_{\text{PGU}} + N_{\text{FR}} + N_{\text{BOILER}}) \times \text{cost}_{\text{NG}} + E_{\text{GRID}} \times \text{cost}_{\text{elect}} \quad (29)$$

351 where E_{GRID} is the electricity purchased from the grid. While cost_{NG} and $\text{cost}_{\text{elect}}$
 352 are the cost of the natural gas and grid electricity, respectively. Also, the amount of
 353 carbon dioxide emitted by the CHP system is determined as Eq. (30).

$$\text{CD}_{\text{Emission}} = (N_{\text{PGU}} + N_{\text{FR}} + N_{\text{BOILER}}) \times \gamma_{\text{NG}} + E_{\text{GRID}} \times \gamma_{\text{GRID}} \quad (30)$$

355 where γ_{NG} and γ_{GRID} are the emission conversion factor of the natural gas and grid,
 356 respectively. Figure 4 presents the flowchart of the harmonized natural gas and fuel
 357 cell CHP system following the hybrid electric-thermal strategy [34].

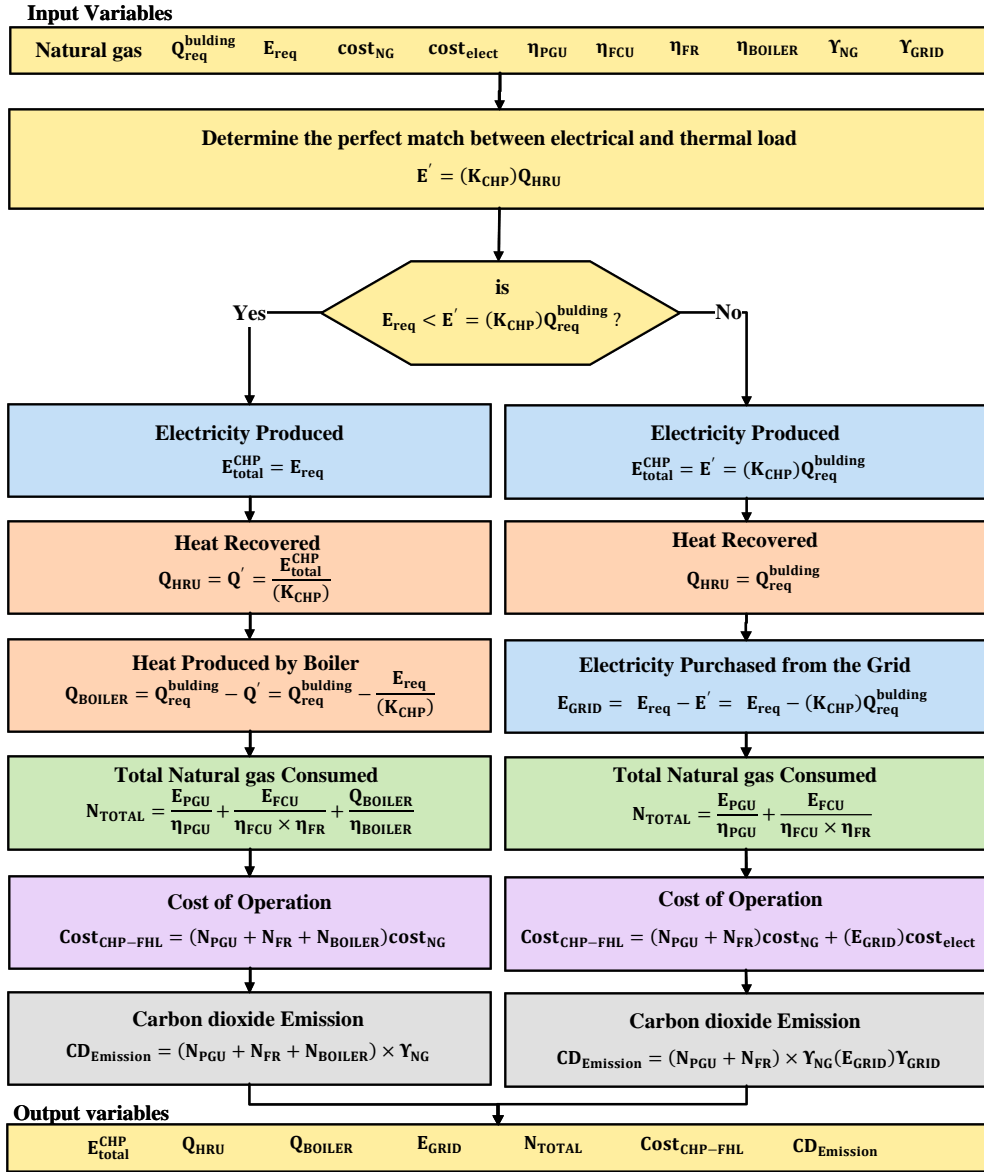


Figure 4: Flowchart of a harmonized natural gas and fuel cell CHP system following the hybrid electric-thermal strategy.

358 2.4. Modelling of G2V and V2G facilities of EVs

359 The modal of EV is indicated by Eqs. (31)-(37). The default charging and dis-
 360 charging periods of EVs to investigate the desired facilities of G2V and V2G can

361 be as follows in Eqs. (31) and (32). These periods can be changed based on the
 363 generated scenarios.

$$365 \quad T_{\text{Ch}}^{\text{Day}} = \{1, 2, \dots, 6\} \Rightarrow \text{G2V operation} \quad (31)$$

$$364 \quad T_{\text{Dch}}^{\text{Day}} = \{18, 19, \dots, 24\} \Rightarrow \text{V2G operation} \quad (32)$$

367 where $T_{\text{Charge}}^{\text{Day}}$ and $T_{\text{Discharge}}^{\text{Day}}$ are the time of day in hours that EVs allowed to be
 368 charge or discharge. In other words, the arrival and departure times of EVs in the
 369 charging station are related to their charging and discharging times. The energy
 370 balance of EV batteries is formulated by Eq. (33).
 371

$$\text{SOC}_t^{\text{EV}} = \text{SOC}_{t-1}^{\text{EV}} + (P_t^{\text{EV}+} \cdot \eta^{\text{EV}-} - P_t^{\text{EV}-} / \eta^{\text{EV}-}) / P_{\text{Total}}^{\text{EV}} \quad (33)$$

372 where SOC_t^{EV} is the EV's battery state of charge (SoC) at time t, $P_t^{\text{EV}+}$ and $P_t^{\text{EV}-}$ are
 374 the charging and discharging energies in the EV battery at time t, respectively, and
 375 $P_{\text{Total}}^{\text{EV}}$ is the total energy that can be stored in the EV battery (EV battery capacity).
 376 At any given time, the SoC of EV batteries must be in its allowed capacity as shown
 377 in Eq. (34).
 378

$$\underline{\text{SOC}}^{\text{EV}} \leq \text{SOC}_t^{\text{EV}} \leq \overline{\text{SOC}}^{\text{EV}} \quad (34)$$

379 where $\underline{\text{SOC}}^{\text{EV}}$ and $\overline{\text{SOC}}^{\text{EV}}$ are the minimum and maximum SoC of the EV bat-
 381 tery, respectively. Eqs. (35) and (36) demonstrate the upper/lower limits of charg-
 382 ing/discharging of EV battery.
 383

$$385 \quad 0 \leq P_t^{\text{EV}+} \leq P_{\text{Total}}^{\text{EV}} \cdot (1 - \text{SOC}_{t-1}^{\text{EV}}) / \eta^{\text{EV}+} \quad (35)$$

$$384 \quad 0 \leq P_t^{\text{EV}-} \leq P_{\text{Total}}^{\text{EV}} \cdot \text{SOC}_{t-1}^{\text{EV}} \cdot \eta^{\text{EV}-} \quad (36)$$

387 Besides, each EV should be charged to its targeted SoC during the departure
 388 period (charging period) as represented by Eq. (37) [36].
 389

$$\text{SOC}_{t_{\text{Dep}}}^{\text{EV}} = \text{SOC}^{\text{EV, Dep}} \quad (37)$$

390

391 *2.5. Modelling wind turbine*

392 The effective power produced by the wind turbine to feed into the MG network
393 can be estimated based on Eqs. (38)-(40).
394

$$395 \quad P_{\text{eff}}^{\text{WT}} = 1/2 \times (\eta_{\text{WT}} \cdot \rho \cdot A \cdot \bar{C}^3) \quad (38)$$

$$396 \quad \eta_{\text{WT}} = C_p \cdot \eta_{\text{gear}} \cdot \eta_{\text{gen}} \eta_{\text{elec}} \quad (39)$$

$$397 \quad A = \pi \cdot [(l_{\text{WT}} + r_{\text{WT}})^2 - (r_{\text{WT}})^2] = \pi \cdot l_{\text{WT}}(l_{\text{WT}} + 2 \cdot r_{\text{WT}}) \quad (40)$$

397 where ρ is the density of air, A is the swept area of the wind turbine blades, \bar{C} is the
398 average wind speed over a specified period, C_p is the power coefficient, while η_{gear} ,
399 η_{gen} and η_{elec} are the efficiency of the gearbox, generator, and electric components,
400 respectively. l_{WT} is the length of the wind turbine blades, and r_{WT} is the wind
401 turbine hub's radius. In addition, the wind speed variation at the selected wind
402 turbine site can be described using the Weibull distribution function [37]. Hence,
403 the probability density function of the Weibull variable \bar{C} is defined as Eq. (41).
404

$$405 \quad f(\bar{C}, k, \lambda) = \begin{cases} \frac{k}{\lambda} \left(\frac{\bar{C}}{\lambda}\right)^{k-1} \cdot \exp\left(-\left(\frac{\bar{C}}{\lambda}\right)^k\right) & \bar{C} \geq 0 \\ 0 & \bar{C} < 0 \end{cases} \quad (41)$$

405 where k and λ are the shape factor and scale factor, respectively. The shape factor
406 measures the width of the distribution, while the scale factor relates closely to the
407 average wind speed. The value of the Weibull's shape factor (k) and Weibull's scale
408 factor (λ) changes with respect to the selected site's wind profile [38].

409 *2.6. Modelling PV arrays*

410 The power produced by the PV panels is defined as Eq. (42).
411

$$412 \quad P_t^{\text{PV}} = \frac{E_t^{\text{PV}}}{t} = \frac{N_{\text{Total}}^{\text{PV}} \times A \times \eta \times H \times \text{PR}}{t} \quad (42)$$

412 where $N_{\text{Total}}^{\text{PV}}$ is the total number of PV panels, A is the area of each PV panel, η is the
413 PV panel's efficiency, H is the amount of solar radiation hitting the panel, and PR
414 is the panel's performance ratio or coefficient losses. Also, the temperature of the
415 panels and the average energy produced by the PV arrays can be estimated based
416 on Eqs. (43) and (44).

417
$$T^{\text{panel}} = T^{\text{amb.}} + \frac{(N_{\text{OT}} - 20)}{0.8} \times H \quad (43)$$

418
$$E_{\text{av.}}^{\text{PV}} = N_{\text{Total}}^{\text{PV}} \times (A \times \eta \times H \times \text{PR}) \quad (44)$$

419 where T^{panel} and $T^{\text{amb.}}$ are the temperature of the panel and ambient temperature,
420 respectively [39].

421 *2.7. Modelling BESS*

422 The incorporated BESS in this design reinforces the RESs due to their inter-
423 mittent nature, stores the excess electrical energy from the CHP technologies, and
424 supports V2G operations during peak demand periods. In addition, the BESS is op-
425 timized to save MG's operating costs and lower CO₂ emissions. Hence, the system
426 stores electrical energy when electricity price and CO₂ emission rates are low, and
427 discharges to meet high demand prices and minimize CO₂ emissions. At any given
428 time, the SOC of BESS should be in its determined limits as indicated in Eq. (45).

429
$$\underline{\text{SOC}}^{\text{BESS}} \leq \text{SOC}_t^{\text{BESS}} \leq \overline{\text{SOC}}^{\text{BESS}} \quad (45)$$

430 where $\text{SOC}_t^{\text{BESS}}$ is the BESS state of charge at time t , $\underline{\text{SOC}}^{\text{BESS}}$ and $\overline{\text{SOC}}^{\text{BESS}}$ are the
431 minimum and maximum state of charge of the BESS, respectively. The maximum
432 power required to charge the BESS can be defined as Eq. (46).

433
$$\overline{P}_t^{\text{BESS+}} = \frac{(\text{SOC}_t^{\text{BESS}} - \underline{\text{SOC}}^{\text{BESS}}) \times E_{\text{Total}}^{\text{BESS}}}{t} > 0 \quad (46)$$

434 $E_{\text{Total}}^{\text{BESS}}$ is the total electrical energy that can be stored in the BESS [40].

435 *2.8. Modelling MG power demand*

436 The MG network design consists of CHP technologies, WT, PV arrays, and BESS
437 integrated into the power distribution network to support EVs' G2V and V2G op-
438 erations as well as the power demand. The power balance formulation can be ex-
439 pressed as Eq. (47).

440
$$P_t^{\text{EV+}} - P_t^{\text{EV-}} = P_t^{\text{CHP}} + P_t^{\text{PV}} + P_t^{\text{WT}} + P_t^{\text{BESS-}} - P_t^{\text{BESS+}} + P_t^{\text{grid-}} - P_t^{\text{grid+}} - P_t^{\text{Load}} \quad (47)$$

441

442 where P_t^{EV+} and P_t^{EV-} are the power required to charge the EVs and power discharge
443 to the grid at time t , respectively. P_t^{CHP} , P_t^{PV} , P_t^{WT} are the power produced by the
444 CHP, PV and WT, respectively. P_t^{BESS-} and P_t^{BESS+} are the discharge and charge power
445 of the BESS, respectively. Also, P_t^{grid-} and P_t^{grid+} are indicates the power purchased
446 from the electricity grid and power sell to the electricity grid, respectively. P_t^{Load} is
447 the power demand of the MG. If P_t^{Load} is assumed to be zero, four operation schemes
448 can be considered in meeting the EVs' power demand.

449 **Scheme 1:** The power produced by the CHP, PV and WT meets the EVs' power
450 demand as shown in Eqs. (48) and (49).
451

$$452 \quad P_t^{EV+} = (P_t^{CHP} + P_t^{PV} + P_t^{WT}) \quad (48)$$

$$453 \quad P_t^{BESS\pm} = 0, \quad P_t^{grid\pm} = 0 \quad (49)$$

454 **Scheme 2:** The power produced by CHP, PV and WT exceeds the EVs' power de-
455 mand as shown in Eq. (50).

$$456 \quad P_t^{EV+} < (P_t^{CHP} + P_t^{PV} + P_t^{WT}) \quad (50)$$

457 when:

$$458 \quad E_t^{BESS} < E_{Total}^{BESS} \quad \text{and} \quad \bar{P}^{BESS+} \geq (P_t^{CHP} + P_t^{PV} + P_t^{WT}) - P_t^{EV+} \quad (51)$$

459 Then:

$$460 \quad P_t^{grid+} = (P_t^{CHP} + P_t^{PV} + P_t^{WT}) - (P_t^{EV+} + P_t^{BESS+}) = 0 \quad (52)$$

$$461 \quad P_t^{BESS+} = \frac{SOC_t^{BESS} \times E_{Total}^{BESS}}{t} \quad (53)$$

462 Eq. (52) indicates that no power is sold to the grid and Eq. (53 shows
463 the power required to charge the BESS.

464 when:

$$465 \quad E_t^{BESS} = E_{Total}^{BESS} \quad (54)$$

466 Then:

$$467 \quad SOC_t^{BESS} = \frac{1}{1} \times 100 = 100\% \quad (55)$$

467

$$P_t^{\text{grid}^+} = (P_t^{\text{CHP}} + P_t^{\text{PV}} + P_t^{\text{WT}}) - (P_t^{\text{EV}^+} + P_t^{\text{BESS}^+}) > 0 \quad (56)$$

468

Eq. (54) indicates that BESS is fully charged and Eq. (55) shows the

469

amount of power sold to the grid.

470

Scheme 3: The power produced by CHP, PV and WT does not meet the EVs' power demand as shown in Eq. (57).

471

472

$$P_t^{\text{EV}^+} > (P_t^{\text{CHP}} + P_t^{\text{PV}} + P_t^{\text{WT}}) \quad (57)$$

473

when:

474

$$\text{SOC}_t^{\text{BESS}} > \underline{\text{SOC}}^{\text{BESS}} \quad (58)$$

475

Then:

476

$$\bar{P}_t^{\text{BESS}^-} = \frac{\text{SOC}_t^{\text{BESS}} - \underline{\text{SOC}}^{\text{BESS}} \times E_{\text{Total}}^{\text{BESS}}}{t} > 0 \quad (59)$$

477

Eq. (59) indicates the maximum power supplied by BESS.

478

when:

479

$$\text{SOC}_t^{\text{BESS}} = \underline{\text{SOC}}^{\text{BESS}} \quad \text{or} \quad \bar{P}_t^{\text{BESS}^-} < P_t^{\text{EV}} - (P_t^{\text{CHP}} + P_t^{\text{PV}} + P_t^{\text{WT}}) \quad (60)$$

480

Then:

481

$$P_t^{\text{grid}^-} = P_t^{\text{EV}^+} - (P_t^{\text{CHP}} + P_t^{\text{PV}} + P_t^{\text{WT}}) > 0 \quad (61)$$

482

Eq. (61) shows the amount of power purchased from the grid.

483

Scheme 4: The power produced by the CHP, PV and WT does not meet the EVs' power demand, and the power purchased from the grid is insufficient.

484

In this scheme, Eqs. (62) and (63) can be presented.

485

486

$$P_t^{\text{EV}^+} > (P_t^{\text{CHP}} + P_t^{\text{PV}} + P_t^{\text{WT}}) + (\bar{P}_t^{\text{BESS}^-} + P_t^{\text{grid}^-}) \quad (62)$$

487

$$P_t^{\text{EPNM}} = \sum P_t^{\text{EV}} - \sum (P_t^{\text{CHP}} + P_t^{\text{PV}} + P_t^{\text{WT}} + P_t^{\text{grid}^-} + \bar{P}_t^{\text{BESS}^-}) > 0 \quad (63)$$

488

Eq. (62) indicates that the system has power deficit and Eq. (63) shows

489

the amount of expected power not met [41].

490 3. Objective functions and constraints

491 The objective function aims to minimize the operating costs and CO₂ emissions
 492 in the MG connected network's G2V and V2G operations of EVs as shown in Eq. (64).

$$\min \text{OB}_{\text{function}} = \sum_s \mu_s [\text{OP}_{\text{cost}} + (\lambda^{\text{CO}_2}) \text{CD}_{\text{emission}}] \quad (64)$$

493 where OP_{cost} is the operating cost function and $\text{CD}_{\text{emission}}$ is the emission func-
 494 tion. μ_s is the probability of scenario s . To equalize the dimensions of these two
 495 items within the objective function, the price of CO₂ emissions per kg, λ^{CO_2} , is mul-
 496 tiplied by the emission function [42].

499 3.1. Operating cost function

500 The total operating cost of the MG enabling the G2V and V2G operations can
 501 be described as Eq. (65).

$$\text{OP}_{\text{cost}} = \text{OP}_{\text{cost}}^{\text{DG}} + \text{OP}_{\text{cost}}^{\text{Batt.}} + \text{OP}_{\text{cost}}^{\text{Grid}}, \quad \forall s \in \{1, \dots, S\} \quad (65)$$

502 where $\text{OP}_{\text{cost}}^{\text{DG}}$ is the operating costs of the distributed generation (CHP, PV and WT),
 503 $\text{OP}_{\text{cost}}^{\text{Batt.}}$ is the operating costs of the batteries (BESS and EV). While $\text{OP}_{\text{cost}}^{\text{Grid}}$ is the cost
 504 of buying or selling power from/to the utility grid.

505 The $\text{OP}_{\text{cost}}^{\text{DG}}$ is defined in Eqs. (66)-(69).

$$\text{OP}_{\text{cost}}^{\text{DG}} = \text{OP}_{\text{cost}}^{\text{CHP}} + \text{OP}_{\text{cost}}^{\text{PV}} + \text{OP}_{\text{cost}}^{\text{WT}}, \quad \forall s \in \{1, \dots, S\} \quad (66)$$

$$\text{OP}_{\text{cost}}^{\text{CHP}} = \sum_t^T P_{t,s}^{\text{CHP}} \times \lambda_t^{\text{CHP}}, \quad \forall s \in \{1, \dots, S\} \quad (67)$$

$$\text{OP}_{\text{cost}}^{\text{PV}} = \sum_t^T P_{t,s}^{\text{PV}} \times \lambda_t^{\text{PV}}, \quad \forall s \in \{1, \dots, S\} \quad (68)$$

$$\text{OP}_{\text{cost}}^{\text{WT}} = \sum_t^T P_{t,s}^{\text{WT}} \times \lambda_t^{\text{WT}}, \quad \forall s \in \{1, \dots, S\} \quad (69)$$

515 where $\text{OP}_{\text{cost}}^{\text{CHP}}$, $\text{OP}_{\text{cost}}^{\text{PV}}$ and $\text{OP}_{\text{cost}}^{\text{WT}}$ are the operating costs of the CHP, PV and WT,
 516 respectively. $P_{t,s}^{\text{CHP}}$, $P_{t,s}^{\text{PV}}$ and $P_{t,s}^{\text{WT}}$ are the power output of the CHP, PV and WT, re-
 517 spectively, at time t for scenario s . While λ_t^{CHP} , λ_t^{PV} and λ_t^{WT} are the utilization costs
 518 of the CHP, PV and WT, respectively.

519 Furthermore, $\text{OP}_{\text{cost}}^{\text{Batt.}}$ and $\text{OP}_{\text{cost}}^{\text{Grid}}$ are defined in Eqs. (70)-(73).

521

$$\text{OP}_{\text{cost}}^{\text{Batt.}} = \text{OP}_{\text{cost}}^{\text{BESS}} + \text{OP}_{\text{cost}}^{\text{EV}}, \quad \forall s \in \{1, \dots, S\} \quad (70)$$

523

522

$$\text{OP}_{\text{cost}}^{\text{BESS}} = \sum_t^T (P_{t,s}^{\text{BESS-}} \times S_t^{\text{BESS}}) - (P_{t,s}^{\text{BESS+}} \times B_t^{\text{grid}}), \quad \forall s \in \{1, \dots, S\} \quad (71)$$

525

524

$$\text{OP}_{\text{cost}}^{\text{EV}} = \sum_t^T (P_{t,s}^{\text{EV-}} \times S_t^{\text{EV}}) - (P_{t,s}^{\text{EV+}} \times B_t^{\text{grid}}), \quad \forall s \in \{1, \dots, S\} \quad (72)$$

527

526

$$\text{OP}_{\text{cost}}^{\text{Grid}} = \sum_t^T (P_{t,s}^{\text{grid-}} \times B_t^{\text{grid}}) - (P_{t,s}^{\text{grid+}} \times S_t^{\text{grid}}), \quad \forall s \in \{1, \dots, S\} \quad (73)$$

528

529

530

531

532

533

534

535

where $\text{OP}_{\text{cost}}^{\text{BESS}}$ and $\text{OP}_{\text{cost}}^{\text{EV}}$ are the operating costs of the BESS and EV. $P_{t,s}^{\text{BESS-}}$, $P_{t,s}^{\text{EV-}}$ and $P_{t,s}^{\text{grid-}}$ are the power supplied by BESS, EV and grid at time t for scenario s . $P_{t,s}^{\text{BESS+}}$ and $P_{t,s}^{\text{EV+}}$ are the power for charging the BESS and EV at time t for scenario s . $P_{t,s}^{\text{grid+}}$ is the excess power sold to the utility grid at time t for scenario s . While S_t^{BESS} , S_t^{EV} and S_t^{grid} are the costs of selling power from the BESS, EV and grid, respectively. B_t^{grid} is the cost of buying power from the grid to either charge the BESS, EV or supply the MG power demand.

536 3.2. Emission function

537

538

539

540

541

The proposed emission function consists of the GHG emissions from the PV, WT, CHP unit, and the emissions arising out of the power purchased from the utility grid. Hence, the emission function is expressed as in Eqs. (74)-(78).

542

$$\text{CD}_{\text{EM}} = \text{EM}_{\text{PV}} + \text{EM}_{\text{WT}} + \text{EM}_{\text{CHP}} + \text{EM}_{\text{Grid}} \quad \forall s \in \{1, \dots, S\} \quad (74)$$

542

541

$$\text{EM}_{\text{PV}} = \sum_t^T P_{t,s}^{\text{PV}} \times \gamma_t^{\text{PV}}, \quad \forall t \in \{1, \dots, T\} \quad \text{and} \quad \forall s \in \{1, \dots, S\} \quad (75)$$

544

543

$$\text{EM}_{\text{WT}} = \sum_t^T P_{t,s}^{\text{WT}} \times \gamma_t^{\text{WT}}, \quad \forall t \in \{1, \dots, T\} \quad \text{and} \quad \forall s \in \{1, \dots, S\} \quad (76)$$

546

545

$$\text{EM}_{\text{CHP}} = \sum_t^T P_{t,s}^{\text{CHP}} \times \gamma_t^{\text{CHP}}, \quad \forall t \in \{1, \dots, T\} \quad \text{and} \quad \forall s \in \{1, \dots, S\} \quad (77)$$

548

547

$$\text{EM}_{\text{Grid}} = \sum_t^T P_{t,s}^{\text{grid-}} \times \gamma_t^{\text{grid}}, \quad \forall t \in \{1, \dots, T\} \quad \text{and} \quad \forall s \in \{1, \dots, S\} \quad (78)$$

549

550

551

552

where EM_{PV} , EM_{WT} , EM_{CHP} , and EM_{Grid} are CO₂ emissions from the PV, WT, CHP unit, and utility grid, respectively. γ_t^{PV} , γ_t^{WT} , γ_t^{CHP} , and γ_t^{grid} are CO₂ emission rate of the PV, WT, CHP unit, and grid, respectively.

553 *3.3. Grid distribution line constraint*

554 There is a limit on the maximum apparent power that can flow through the
 555 distribution lines due to their rated voltage and cross-sectional areas as Eq. (79).
 556

$$|P_{t,s}^{\text{flow}}| \leq |\bar{P}^{\text{flow}}|, \quad \forall t \in \{1, \dots, T\} \text{ and } \forall s \in \{1, \dots, S\} \quad (79)$$

559 where $P_{t,s}^{\text{flow}}$ is the apparent power flowing through the distribution lines at time t
 559 for scenario s , \bar{P}^{flow} is the maximum power that can flow through the lines.

560 *3.4. Voltage limit*

561 At any bus of the MG distribution network, the following voltage limit should
 562 be observed as Eq. (80).
 563

$$\underline{V}^i \leq V_{t,s}^i \leq \bar{V}^i, \quad t = \{1, 2, \dots, T\} \text{ and } \forall s \in \{1, \dots, S\} \quad (80)$$

565 where \underline{V}^i and \bar{V}^i are the minimum and maximum voltage boundary, respective.
 566 $V_{t,s}^i$ is the voltage of bus i at time t for scenario s .

567 *3.5. Battery charging and discharging constraint*

568 The EVs' batteries and power-packs of the BESS work within permitted charging
 569 and discharging limits that must be upheld as shown in Eqs. (81)-(82).
 570

$$P_{t,s}^{i+} \leq P_{\text{limit}}^{i+} \times C_{t,s}^i, \quad i = \text{EV or BESS} \quad \forall t \in \{1, \dots, T\}, \quad \forall s \in \{1, \dots, S\}, \quad C \in \{0, 1\} \quad (81)$$

$$P_{t,s}^{i-} \leq P_{\text{limit}}^{i-} \times D_{t,s}^i, \quad i = \text{EV or BESS} \quad \forall t \in \{1, \dots, T\}, \quad \forall s \in \{1, \dots, S\}, \quad D \in \{0, 1\} \quad (82)$$

574 where P_{limit}^{i+} and P_{limit}^{i-} are the charging and discharging limits of the batteries, re-
 575 spectively. C and D are the binary variables for specifying the charging and dis-
 576 charging of the batteries at any given time, t . C and D are within the boundary of 0
 577 and 1. Furthermore, the respective batteries of the EV and BESS cannot be charged
 578 and discharged concurrently. This constraint is expressed as Eq. (83).
 579

$$C_{t,s}^i + D_{t,s}^i \leq 1, \quad i = \text{EV or BESS} \quad \forall t \in \{1, \dots, T\}, \quad \forall s \in \{1, \dots, S\}, \quad C, D \in \{0, 1\} \quad (83)$$

580

581 3.6. Power balance

582 The total power supplied by the connected electricity grid and distributed power
 583 generating sources must equal the total power demand at each time t for each sce-
 584 nario s as demonstrated in Eq. (84).
 585

$$p_{t,s}^{CHP} + p_{t,s}^{PV} + p_{t,s}^{WT} + p_{t,s}^{BESS-} + p_{t,s}^{grid-} + p_{t,s}^{EV-} = p_{t,s}^{EV+} + p_{t,s}^{Load} + p_{t,s}^{grid+}, \quad (84)$$

$$\forall t \in \{1, \dots, T\}, \forall s \in \{1, \dots, S\}$$

586

587 4. Test System

588 Figure 5 illustrates the test system design. The system consists of CHP, PV, WT,
 589 and BESS integrated with the power distribution network to provide the energy
 590 required to charge the EVs and supply other loads in the system. In addition, the
 591 V2G strategy is operated to support the grid during the peak demand periods.

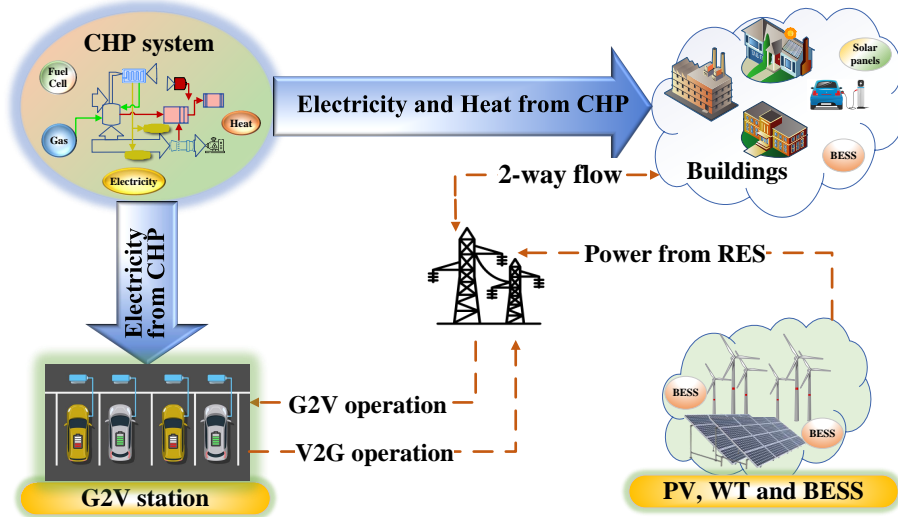


Figure 5: G2V and V2G operations with CHP technologies, RES, and BESS.

592 4.1. Load forecast

593 Figure 6 presents the hourly average load forecast employed in the test system.
 594 Along with the EV loads, the power generated from the CHP, PV and WT supplies
 595 MG power demand through the connected power distribution network.

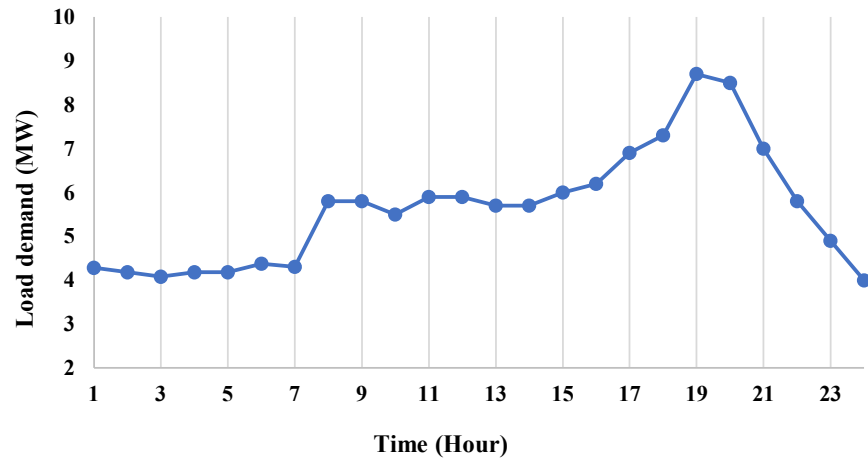


Figure 6: Hourly average load demand.

596 *4.2. CHP specifications*

597 The CHP technologies are designed to provide about 50% to 70% of the system's
 598 hourly power load demand. The by-product heat could be utilized in buildings
 599 or other industrial processes. It should be noted that the heating demand is not
 600 taken into account in this paper and the heat generated by CHP units considered
 601 as a by-product energy. Furthermore, the amount of CHP CO₂ emission during
 602 manufacturing process and operation process is assumed to be 1.5 kg CO₂eq/MWh
 603 and 235 kg CO₂eq/MWh [43]. Table 2 highlights the input values applied in the
 604 CHP unit.

605 *4.3. WT specifications and wind resource*

606 A 2 MW wind turbine with a doubly fed induction generator is chosen for the test
 607 system. In addition, North East of England is selected as the installation location
 608 and has average wind speed data presented in Figure 7 [44]. Furthermore, the
 609 carbon footprint in the life cycle of wind turbines is taken into consideration and the
 610 amount of WT CO₂ emission during manufacturing process and operation process
 611 is assumed to be 11 kg CO₂eq/MWh and 1 kg CO₂eq/MWh [45]. Table 3 highlights
 612 the key specifications of the selected wind turbine.

Table 2: Input values for CHP units.

Variables	Symbol	Values
Gas turbine (GT) rating	-	4 MW
Fuel cell unit (FCU) rating	-	2 MW
Efficiency of GT	η_{PGU}	48.3%
Efficiency of FCU	η_{FCU}	60%
Efficiency of fuel reformer	η_{FR}	74%
Efficiency of heat recovery unit	η_{HRU}	80%
Efficiency of heating coil	η_{HC}	80%
Efficiency of boiler	η_{BOILER}	94%
Price of natural gas	$cost_{NG}$	£4.88/MMBtu
Natural gas emission rate	Em_{NG}	150 kg CO ₂ /MWh

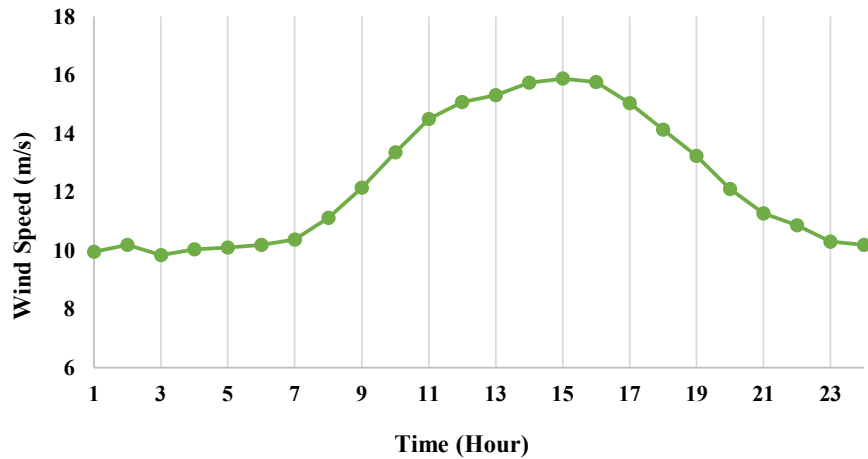


Figure 7: Hourly average wind speed for North East England.

613 4.4. PV specifications and solar resource

614 A 380 W PV panel is used in the test system. The PV panel is designed to optimize
615 energy generation and has a product and power coverage warranty of 40 years. In
616 addition, the carbon footprint of PV during manufacturing process and operation

Table 3: Wind turbine specifications [46].

Specifications	Values
Rated generator output	2000 kW
Diameter	80 m
Swept area	4978 m ²
Blade length	39 m
Cut-in wind speed	4 m/s
Cut-out wind speed	25 m/s

617 process is assumed to be 12 kg CO₂eq/MWh and 27 kg CO₂eq/MWh [47]. Table 4
 618 shows the PV's key specifications, and Figure 8 presents the hourly solar irradiance
 619 of the selected installation site, North East England [48].

620 4.5. EV and BESS specifications

621 Only a few EVs are currently built to support V2G operations. Hence, the Kia
 622 Soul EV is selected for the test system. Conversely, the Tesla power-pack is used
 623 for the BESS. The BESS is installed to support V2G operation during peak demand,
 624 reduce the intermittent nature of the added RESs and minimize energy wastage
 625 by storing the excess energy from the CHP and electricity grid. Also, the BESS is
 626 configured to a minimum and maximum state of charge (SoC) of 10% and 95%,
 627 respectively. Table 5 and Table 6 highlight the chosen EV and power-pack specifi-
 628 cations, respectively.

629 4.6. Grid supply and electricity prices

630 The test system design is integrated with the power distribution network for easy
 631 and low-cost evacuation of the power generated from the CHP, PV, and WT. Also,
 632 the distribution network acts as a medium for the sales or purchase of excess or
 633 shortage power, respectively. Therefore, the average hourly price of grid electricity
 634 for North East England is deployed in the test system. Figure 9 shows the grid
 635 electricity prices [49] and CO₂ emissions [50].

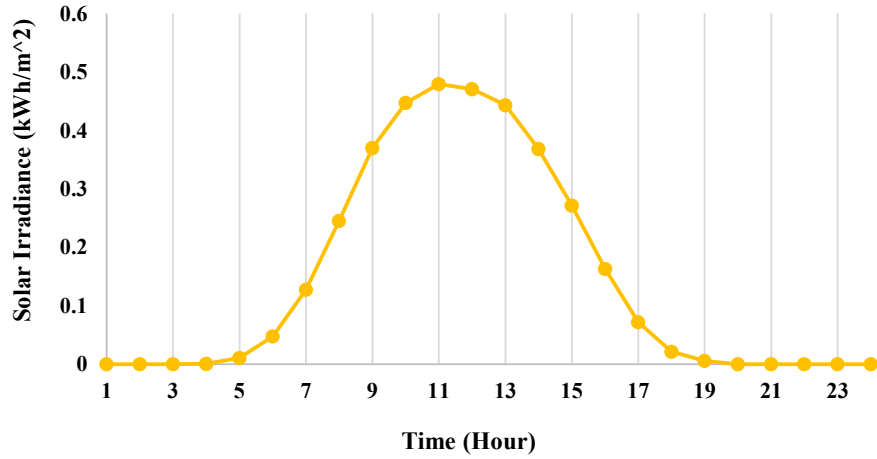


Figure 8: Hourly average solar irradiance for North East England.

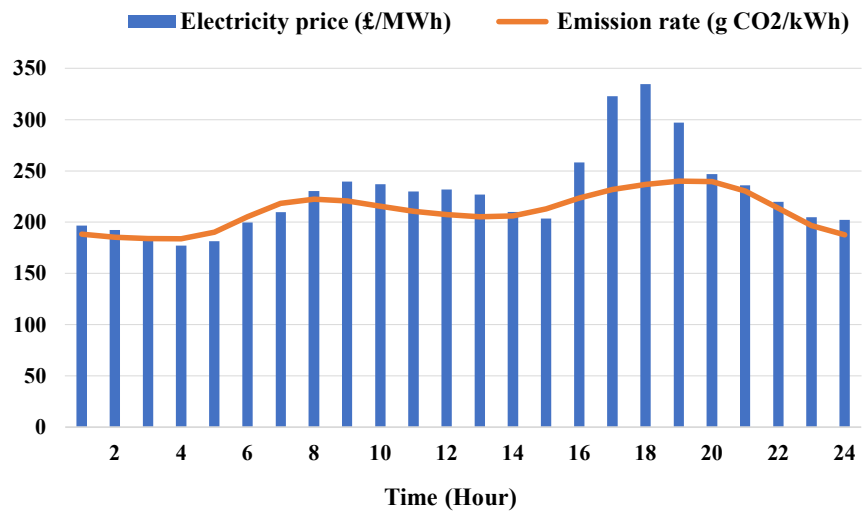


Figure 9: Hourly electricity prices and CO₂ emission rates for North East England.

636 **5. Results and Discussions**

637 For the sake of a detailed analysis, four case studies (CSs) are defined in this
 638 paper as follows:

Table 4: PV panels specifications [51].

Specifications	Values
Material	Monocrystalline
Maximum annual degradation	25%
Nominal power	380 W
Panel efficiency	21.5%
Panel area	1.76 m ²

Table 5: EV specifications [52].

Specifications	Values
Battery	64 kWh Li-ion polymer battery
Maximum power	150 kW
AC charge time (230 V)	29hrs (0% → 100%)
AC charge time (7.2 kW)	9hrs 35mins (0% → 100%)
DC charge time (50 kW)	1hr 15mins (0% → 80%)
DC charge time (100 kW)	54mins (0% → 80%)
Battery	64 kWh Li-ion polymer battery

Table 6: BESS specifications [52].

Specifications	Values
Depth of discharge	100%
Energy capacity	Up to 232 kWh (AC)
Power	Up to 130 kW (AC)
Scalable inverter power	70 kVA to 700 kVA (at 480 V)
System efficiency	88% round trip (2 hours system)
	89.5% round trip (5 hours system)

639 5.1. CS0

640 In CS0, electricity from the existing power distribution network supplies the EVs
641 and forecasted MG power demand. Hence, the electricity prices and CO₂ emission
642 rates applied are for the utility grid. Figure 10 illustrates the hourly operating cost
643 and CO₂ emission cost in this test case and forms the reference base for other test
644 cases in this research. There are no operational costs or CO₂ minimization under
645 this CS, as both objective functions are driven solely by the set prices of the utility
646 operators, hourly load demands and the types of power generating plants installed
647 upstream. Therefore, the daily average operating and CO₂ emission costs in this CS
648 are approximately £31,820 and £2,898, respectively.

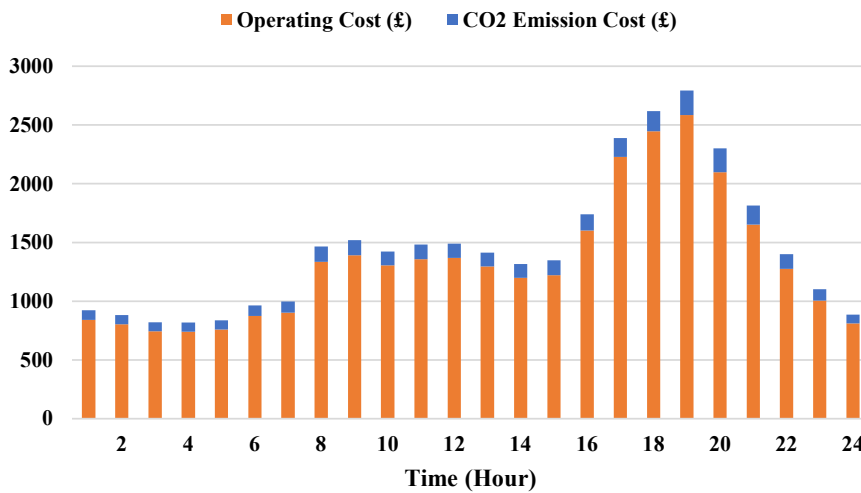


Figure 10: Operating and CO₂ Emission Costs in CS0.

649 5.2. CS1: Only CHP

650 This CS investigates the impacts of deploying the harmonized natural gas and
651 hydrogen fuel cell CHP technologies in facilitating the G2V operations of the EVs in
652 addition to the MG power demand. Firstly, the CHP is operated in an islanded mode
653 (without grid integration) to achieve a better impact system analysis. Lastly, it is
654 used and analyzed in a grid-connected mode. Hence, Figure 11 presents hourly

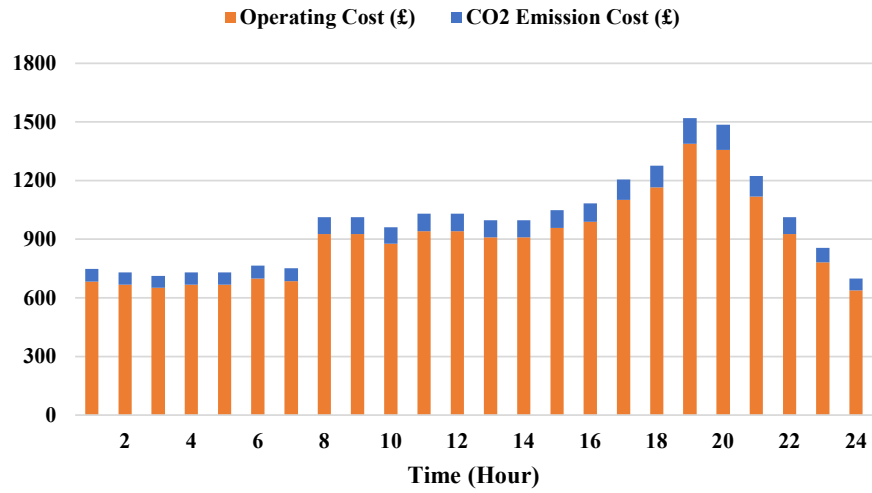
655 operating costs and CO₂ emission costs in the islanded and grid-connected oper-
656 ating modes. In comparing the CHP's operations in the islanded mode with **CS0**,
657 the daily operating costs declined to around £21,568.1, which represents a 32.22%
658 reduction, while the CO₂ emissions plummeted to £2,053.6, a 29.13% decrease
659 in reference to **CS0**. Similarly, 23.00% and 20.89% reductions were achieved in
660 the operating costs and CO₂ emission costs of the grid-connected mode, respec-
661 tively. The lower percentage deduction in the grid-connected mode is due to higher
662 operating costs and CO₂ emissions from the purchased grid power. However, an
663 estimated 659.3 MMBTU/day of heat recovered from the CHP in islanded mode is
664 more than the 622.1 MMBTU/day of heat retrieved in the grid-connected mode,
665 as more power is produced from the CHP to meet the electricity demand, which
666 facilitates the recovery of more by-product heat.

667 5.3. **CS2: With CHP, PV, WT and Grid supply (No BESS)**

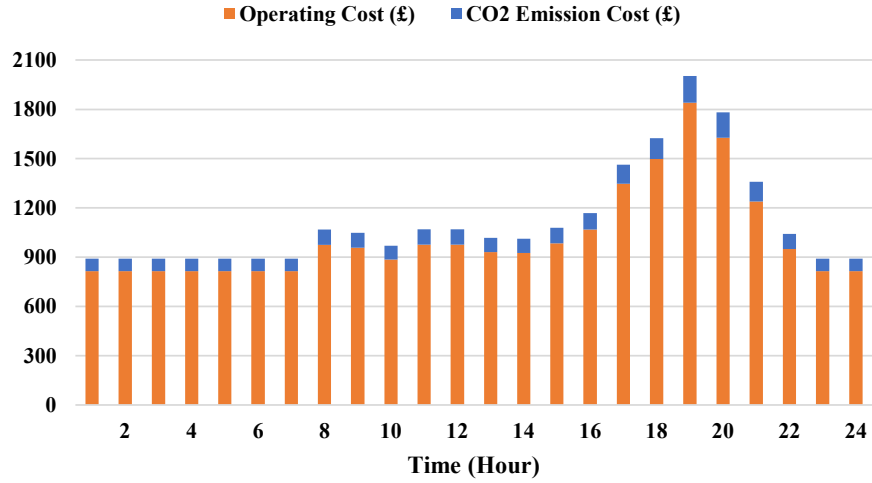
668 **CS2** examines the benefits of adding PV, WT, and national grid to the **CS1**. This
669 approach further minimizes the MG's operating and CO₂ emission costs, as demon-
670 strated in Figure 12. In this CS, the daily operating and emission expenses derived
671 for the MG are about £17,663.8 and £1,532.2. When compared with **CS0**, **CS2**
672 leads to a 44.49% and 47.13% reduction in operating and CO₂ emission costs, re-
673 spectively. Similarly, **CS2** sees an 18.10% and 25.39% decline when set side by
674 side with **CS1** (islanded mode), while 27.90% and 33.16% were achieved when
675 compared with the grid-connected method of **CS1**. Hence, the derived reduction in
676 the two objective functions highlights the impacts of the PV and WT added to the
677 system. Finally, about 365.10 MMBTU/day of heat is recovered from the CHP

678 5.4. **CS3: CS2 and BESS (V2G and G2V operations)- without BESS degradation cost**

679 This CS cross-examines the impacts of the V2G strategy on the MG and the ad-
680 vantages of the BESS in supporting V2G operations. Figure 13 shows the test case's
681 hourly operating and CO₂ emission costs. In this research, the V2G facility is em-
682 ployed for 6 hours a day during the high prices of the electricity. In addition, the
683 BESS primarily acts to support the V2G operations when the power supplied by the



(a) Islanded mode



(b) Grid-connected mode

Figure 11: Operating and CO₂ Emission Costs in CS1 for (a) Islanded mode (b) Grid-connected modes.

684 EV batteries is not enough to meet the MG's high demand. However, the BESS is
 685 also deployed when there is power shortage from the connected utility grid or at
 686 periods of high electricity prices. Conversely, the BESS is charged during hours of
 687 low power demand and low electricity prices. In this CS, the MG operating and CO₂
 688 emission costs declined by 47.20% and 47.90%, respectively, compared to CS0. The
 689 achieved lower minimization values demonstrate the impact of the V2G and BESS
 690 integration. Furthermore, compared with CS1 and CS2, the operating costs plum-
 691 meted by 22.10% and 4.88%, respectively, while the CO₂ emission costs reduced by
 692 26.48% and 1.46%, respectively. Figure 14 compares the CS0, CS1, CS2 and CS3
 693 of the MG operating costs and CO₂ emissions. It is evident that CS3 provides the
 694 best minimization of the objective functions, having achieved total daily operating
 695 costs of around £16,801.67 and daily CO₂ emission costs of £1,509.8.

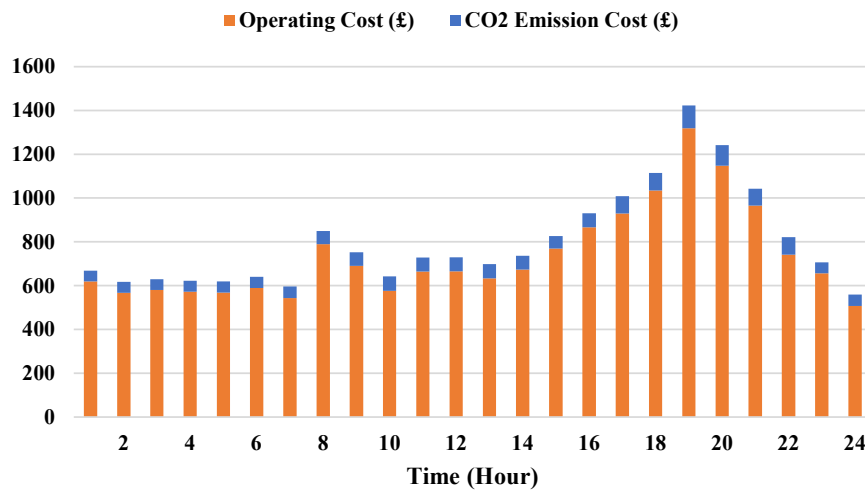


Figure 12: Operating and CO₂ Emission Costs in CS2.

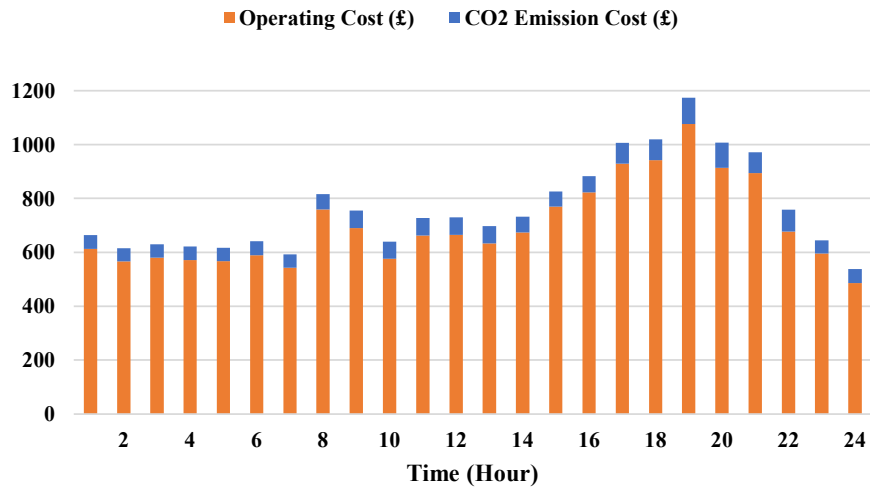
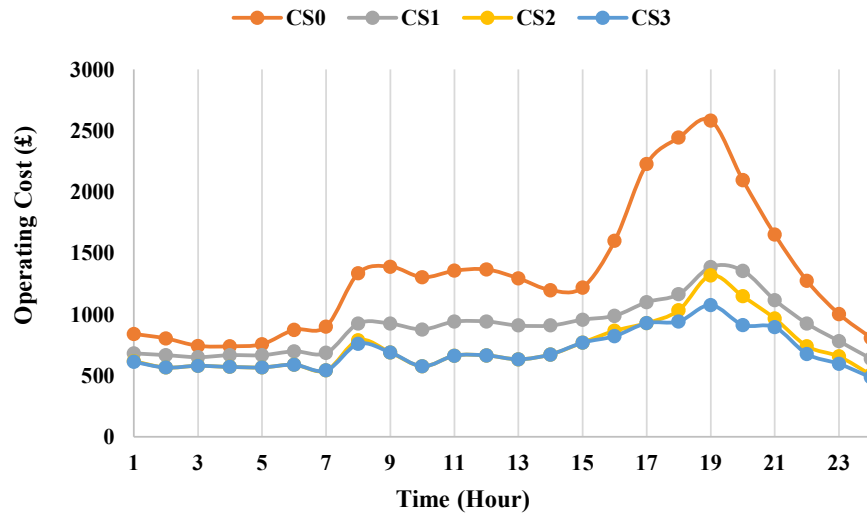


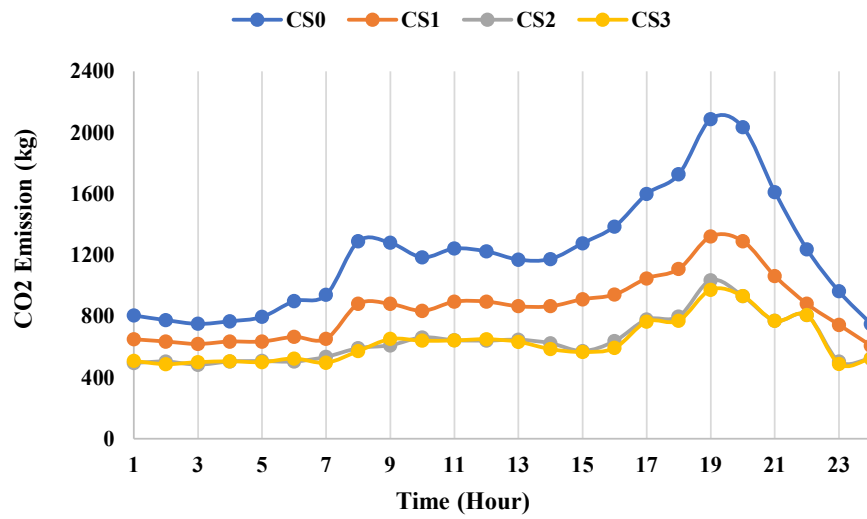
Figure 13: Operating and CO₂ Emission Costs in CS3.

696 5.5. MG power balance

697 Figure 15 presents the power balance for CS3, which considers the whole MG
 698 system consisting of the CHP, PV, WT, BESS, utility grid and V2G strategy. From
 699 the system's power balance, it is observed that the CHP, PV, WT, BESS (V2G oper-
 700 ations), and utility grid contribute an average of 59.16%, 6.11%, 27.54%, 5.11%
 701 and 2.08%, respectively, in meeting the daily power demands for the G2V opera-
 702 tions and forecasted MG power demand. Furthermore, around 14.18% of the daily
 703 generated power from the CHP and RES is sold to the utility grid as excess power,
 704 providing additional revenue for MG's operations.



(a) Operating costs



(b) CO₂ emissions

Figure 14: Comparing (a) Operating costs (b) CO₂ emissions of the CS0, CS1, CS2 and CS3.

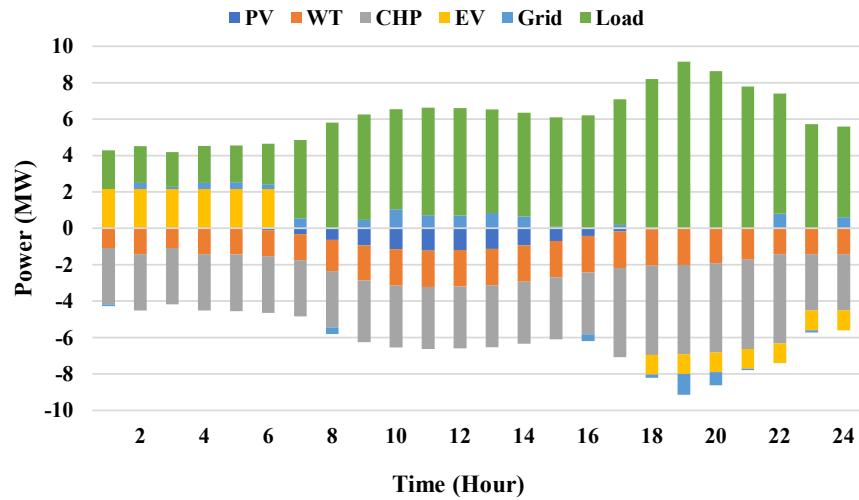


Figure 15: The power balance of the MG network.

705 5.6. LCA Results

706 Figures 16-18 represent the LCA results of the GHG emissions of the PV, WT, and
 707 CHP unit, respectively. It can be noted that 353.13 kg CO₂eq, 489.38 kg CO₂eq, and
 708 20717.41 kg CO₂eq are emitted during a 24-hour time horizon scheduling of the
 709 PV, WT, and CHP unit, respectively. It is clear that applying RES-based units such as
 710 PVs and WTs have a significant impact on reducing global warming factor (CO₂eq)
 711 and the corresponding emission costs.

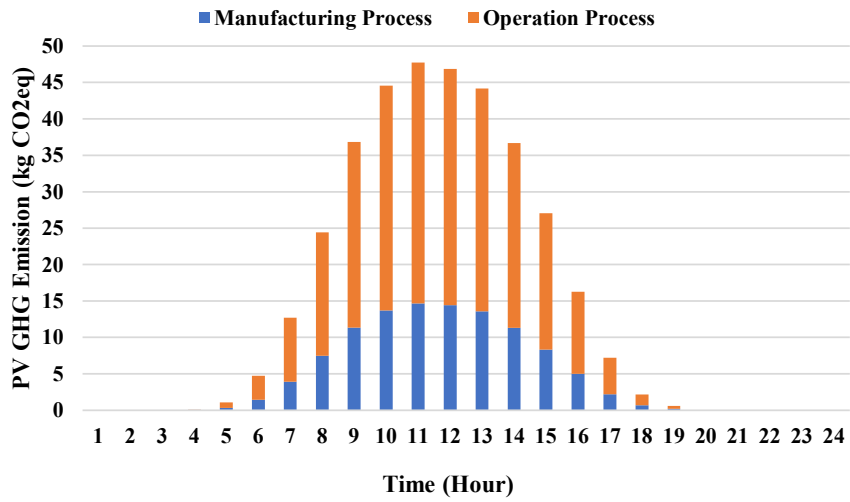


Figure 16: LCA Result for PV GHG Emission.

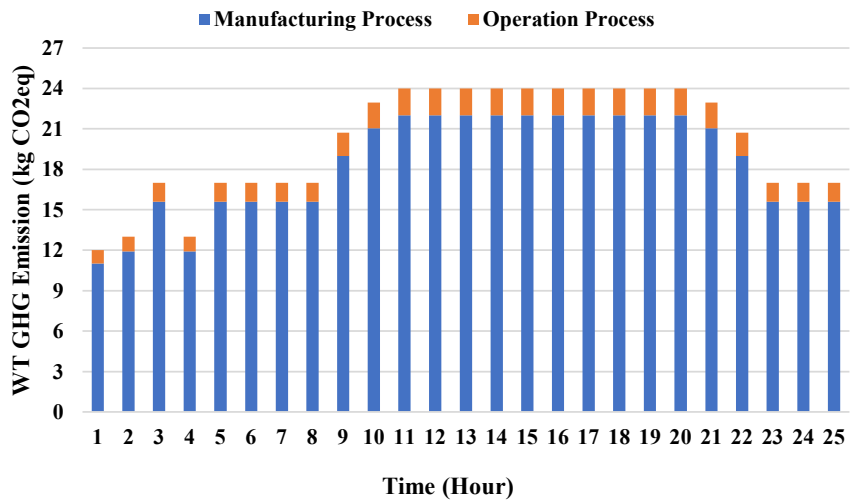


Figure 17: LCA Result for WT GHG Emission.

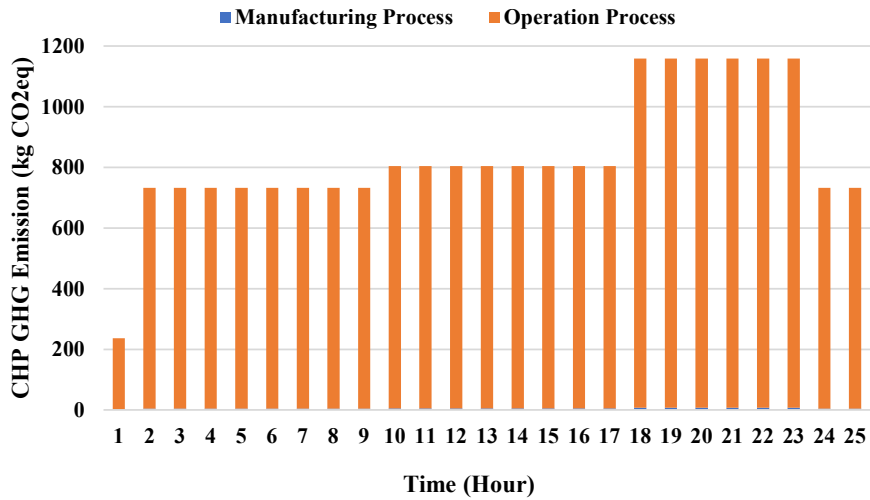


Figure 18: LCA Result for CHP GHG Emission.

712 **6. Conclusion**

713 This paper proposes a stochastic operation of the power distribution networks
 714 via minimizing the operating and CO₂ emissions costs. It examines the integration
 715 multi-energy technologies considering the uncertainties of RES generation, load
 716 consumption, and charging/discharging periods using the scenario-based analysis
 717 method. This paper also successfully analyses the benefits of applying CHP tech-
 718 nologies alongside PV and WT in facilitating the mass deployment of EVs to de-
 719 carbonize the transport sector and contribute to achieving the Net-Zero goal. In
 720 addition, the research provides a complex problem formation of harmonized natu-
 721 ral gas and hydrogen fuel cell CHP technologies following a hybrid electric-thermal
 722 load strategy. Correspondingly, it investigates the integration of BESS in storing the
 723 excess power from the CHP and RES, and supporting the V2G operations of the EVs
 724 at high power demand periods. Furthermore, the research explores the EVs' sched-
 725 uled G2V and V2G strategies. The G2V process happens during base demand pe-
 726 riods at low market prices and CO₂ emissions, while the V2G operation is planned
 727 for high demand periods when the MG's electricity prices and CO₂ emissions are

728 high. Finally, the MG design was tested in four diverse CSs and the LCA impact was
729 investigated to calculate the CO₂ emissions of the distributed generation units.

730 The main results of the simulations are achieved as follows:

- 731 1. In reference to the **CS0**, 23.00% and 20.89% decrease in the MG's operat-
732 ing costs and CO₂ emissions were obtained when deploying only the grid-
733 connected CHP technologies to facilitate the EVs' G2V operations.
- 734 2. Applying the CHP, PV, and WT further reduces the MG's operating costs by
735 44.49% and CO₂ emissions by 47.13%.
- 736 3. Adding the BESS to support the EVs' V2G operations extends the design's
737 impact on the MG's operating costs and CO₂ emissions, lowering them to
738 47.20% and 47.90%, respectively.

739 Therefore, the achieved results showcase the economic and environmental ben-
740 efits of applying CHP technologies with RES and BESS in enabling the mass use of
741 EVs to achieve sustainable decarbonization of the transport sector and contribute to
742 achieving the global Net-Zero goal. According to the architecture of the proposed
743 network, the multi-carrier energy systems can be also studied in future researches.
744 Likewise, multi-energy storage system can be applied in the energy systems to real-
745 ize a comprehensive analysis for the optimal operation of the energy resources. In
746 addition, the self-healing concepts can also be proposed to investigate the operation
747 potentials in the isolated mode.

748 **7. Acknowledgments**

749 This work was supported from DTE Network+ funded by EPSRC grant reference
750 EP/S032053/1.

751 **References**

- 752 [1] A. Hill, L. Martinez-Diaz, Building a Resilient Tomorrow: How to Prepare
753 for the Coming Climate DisruptionHow to Prepare for the Coming Climate
754 Disruption, New York: Oxford University Press, 2020.

- 755 [2] J. Rissman, C. Bataille, E. Masanet, N. Aden, W. R. Morrow, N. Zhou, N. El-
756 liott, R. Dell, N. Heeren, B. Huckestein, J. Cresko, S. A. Miller, J. Roy, P. Fen-
757 nell, B. Cremmins, T. Koch Blank, D. Hone, E. D. Williams, S. de la Rue du
758 Can, B. Sisson, M. Williams, J. Katzenberger, D. Burtraw, G. Sethi, H. Ping,
759 D. Danielson, H. Lu, T. Lorber, J. Dinkel, J. Helseth, Technologies and policies
760 to decarbonize global industry: Review and assessment of mitigation drivers
761 through 2070, *Applied Energy* 266 (2020).
- 762 [3] R. Reitz, H. Ogawa, R. Payri, T. Fansler, S. Kokjohn, Y. Moriyoshi, A. Agar-
763 wal, D. Arcoumanis, D. Assanis, C. Bae, K. Boulouchos, M. Canakci, S. Cur-
764 ran, I. Denbratt, M. Gavaises, M. Guenther, C. Hasse, Z. Huang, T. Ishiyama,
765 B. Johansson, T. Johnson, G. Kalghatgi, M. Koike, S. Kong, A. Leipertz, P. Miles,
766 R. Novella, A. Onorati, M. Richter, S. Shuai, D. Siebers, W. Su, M. Trujillo,
767 N. Uchida, B. Vaglieco, R. Wagner, H. Zhao, *Ijer editorial: The future of the*
768 *internal combustion engine, International Journal of Engine Research* 21 (1)
769 (2020) 3 – 10.
- 770 [4] L. Rivera-González, D. Bolonio, L. F. Mazadiego, S. Naranjo-Silva, K. Escobar-
771 Segovia, Long-term forecast of energy and fuels demand towards a sustain-
772 able road transport sector in ecuador (2016-2035): A leap model application,
773 *Sustainability (Switzerland)* 12 (2) (2020).
- 774 [5] R. Salem, A. Bahadori-Jahromi, A. Mylona, P. Godfrey, D. Cook, Comparison
775 and evaluation of the potential energy, carbon emissions, and financial im-
776 pacts from the incorporation of chp and cchp systems in existing uk hotel
777 buildings, *Energies* 11 (5) (2018).
- 778 [6] M. Alinejad, O. Rezaei, A. Kazemi, S. Bagheri, An optimal management for
779 charging and discharging of electric vehicles in an intelligent parking lot con-
780 sidering vehicle owner’s random behaviors, *Journal of Energy Storage* 35
781 (2021).
- 782 [7] G. Merhy, A. Nait-Sidi-Moh, N. Moubayed, Control, regulation and optimiza-

- 783 tion of bidirectional energy flows for electric vehicles' charging and discharg-
784 ing, *Sustainable Cities and Society* 57 (2020).
- 785 [8] D. Sadeghi, S. E. Ahmadi, N. Amiri, Satinder, M. Marzband, A. Abusorrah,
786 M. Rawa, Designing, optimizing and comparing distributed generation tech-
787 nologies as a substitute system for reducing life cycle costs, co2 emissions, and
788 power losses in residential buildings, *Energy* 253 (2022) 123947.
- 789 [9] S. E. Ahmadi, D. Sadeghi, M. Marzband, A. Abusorrah, K. Sedraoui, Decentral-
790 ized bi-level stochastic optimization approach for multi-agent multi-energy
791 networked micro-grids with multi-energy storage technologies, *Energy* 245
792 (2022) 123223.
- 793 [10] P. Mancarella, Mes (multi-energy systems): An overview of concepts and eval-
794 uation models, *Energy* 65 (2014) 1–17.
- 795 [11] P. Mancarella, G. Andersson, J. Peças-Lopes, K. Bell, Modelling of integrated
796 multi-energy systems: Drivers, requirements, and opportunities, in: 2016
797 Power Systems Computation Conference (PSCC), 2016, pp. 1–22.
- 798 [12] J. Zhao, H. Chang, X. Luo, Z. Tu, S. H. Chan, Dynamic analysis of a cchp system
799 based on fuel cells integrated with methanol-reforming and dehumidification
800 for data centers, *Applied Energy* 309 (2022) 118496.
- 801 [13] L. Fan, Z. Tu, X. Luo, S. H. Chan, Mw cogenerated proton exchange membrane
802 fuel cell combined heat and power system design for eco-neighborhoods in
803 north china, *International Journal of Hydrogen Energy* 47 (6) (2022) 4033–
804 4046.
- 805 [14] J. Zhao, S. Cai, X. Huang, X. Luo, Z. Tu, 4e analysis and multiobjective opti-
806 mization of a pemfc-based cchp system with dehumidification, *Energy Con-
807 version and Management* 248 (2021) 114789.
- 808 [15] S. Cai, X. Li, S. Li, X. Luo, Z. Tu, Flexible load regulation method for a resi-
809 dential energy supply system based on proton exchange membrane fuel cell,
810 *Energy Conversion and Management* 258 (2022) 115527.

- 811 [16] M. Taljegard, L. Göransson, M. Odenberger, F. Johnsson, Impacts of electric
812 vehicles on the electricity generation portfolio – a scandinavian-german case
813 study, *Applied Energy* 235 (2019) 1637 – 1650.
- 814 [17] R. Zhang, S. Fujimori, The role of transport electrification in global climate
815 change mitigation scenarios, *Environmental Research Letters* 15 (3) (2020).
- 816 [18] C. B. Robledo, V. Oldenbroek, F. Abbruzzese, A. J. van Wijk, Integrating a hy-
817 drogen fuel cell electric vehicle with vehicle-to-grid technology, photovoltaic
818 power and a residential building, *Applied Energy* 215 (2018) 615 – 629.
- 819 [19] Z. Liu, Q. Wu, S. Huang, L. Wang, M. Shahidehpour, Y. Xue, Optimal day-
820 ahead charging scheduling of electric vehicles through an aggregative game
821 model, *IEEE Transactions on Smart Grid* 9 (5) (2018) 5173 – 5184.
- 822 [20] B. Sun, Z. Huang, X. Tan, D. H. K. Tsang, Optimal scheduling for electric
823 vehicle charging with discrete charging levels in distribution grid, *IEEE Trans-
824 actions on Smart Grid* 9 (2) (2018) 624 – 634.
- 825 [21] Y. Zhang, P. You, L. Cai, Optimal charging scheduling by pricing for ev charg-
826 ing station with dual charging modes, *IEEE Transactions on Intelligent Trans-
827 portation Systems* 20 (9) (2019) 3386 – 3396.
- 828 [22] R. Das, Y. Wang, G. Putrus, R. Kotter, M. Marzband, B. Herteleer, J. Warmer-
829 dam, Multi-objective techno-economic-environmental optimisation of electric
830 vehicle for energy services, *Applied Energy* 257 (2020) 113965.
- 831 [23] A. Modarresi Ghazvini, J. Olamaei, Optimal sizing of autonomous hybrid pv
832 system with considerations for V2G parking lot as controllable load based on
833 a heuristic optimization algorithm, *Solar Energy* 184 (2019) 30–39.
- 834 [24] M. J. Morshed, J. B. Hmida, A. Fekih, A probabilistic multi-objective approach
835 for power flow optimization in hybrid wind-pv-pev systems, *Applied Energy*
836 211 (2018) 1136–1149.

- 837 [25] J. Zhong, X. Xiong, An orderly ev charging scheduling method based on deep
838 learning in cloud-edge collaborative environment, *Artificial Intelligence and*
839 *Internet of Things (IoT) in Civil Engineering* 184 (2021) 30–39.
- 840 [26] M. Shamshirband, J. Salehi, F. S. Gazijahani, Decentralized trading of plug-in
841 electric vehicle aggregation agents for optimal energy management of smart
842 renewable penetrated microgrids with the aim of CO₂ emission reduction,
843 *Journal of Cleaner Production* 200 (2018) 622–640.
- 844 [27] D. Li, S. Guo, W. He, M. King, J. Wang, Combined capacity and operation opti-
845 misation of lithium-ion battery energy storage working with a combined heat
846 and power system, *Renewable and Sustainable Energy Reviews* 140 (2021)
847 110731.
- 848 [28] Iso 14040:2006 environmental management — life cycle assessment — prin-
849 ciples and framework, <https://www.iso.org/standard/37456.html>.
- 850 [29] R. Turconi, *Life cycle assessment of electricity systems* (2014).
- 851 [30] J. Sadhukhan, S. Sen, S. Gadkari, The mathematics of life cycle sustainability
852 assessment, *Journal of Cleaner Production* 309 (2021) 127457.
- 853 [31] S. E. Ahmadi, N. Rezaei, An igdt-based robust optimization model for opti-
854 mal operational planning of cooperative microgrid clusters: A normal bound-
855 ary intersection multi-objective approach, *International Journal of Electrical*
856 *Power Energy Systems* 127 (2021) 106634.
- 857 [32] H. Heitsch, W. Römisch, Scenario reduction algorithms in stochastic pro-
858 gramming, *Scenario Reduction Algorithms in Stochastic Programming* 24 (2)
859 (2003) 187–206.
- 860 [33] S. E. Ahmadi, N. Rezaei, A new isolated renewable based multi microgrid
861 optimal energy management system considering uncertainty and demand re-
862 sponse, *International Journal of Electrical Power Energy Systems* 118 (2020)
863 105760.

- 864 [34] P. J. Mago, L. M. Chamra, Analysis and optimization of cchp systems based on
865 energy, economical, and environmental considerations, *Renewable and Sus-*
866 *tainable Energy Reviews* 40 (2009) 1099–1106.
- 867 [35] P. Mago, L. Chamra, J. Ramsay, Micro-combined cooling, heating and power
868 systems hybrid electric-thermal load following operation, *Applied Thermal*
869 *Engineering* 30 (8) (2010) 800–806.
- 870 [36] S. E. Ahmadi, M. Marzband, A. Ikpehai, A. Abusorrah, Optimal stochastic
871 scheduling of plug-in electric vehicles as mobile energy storage systems for
872 resilience enhancement of multi-agent multi-energy networked microgrids,
873 *Journal of Energy Storage* 55 (2022) 105566.
- 874 [37] P. Fazlalipour, M. Ehsan, B. Mohammadi-Ivatloo, Risk-aware stochastic bid-
875 ding strategy of renewable micro-grids in day-ahead and real-time markets,
876 *Energy* 171 (2019) 689 – 700.
- 877 [38] A novel falling model for wind speed probability distribution of wind farms,
878 *Renewable Energy* 184 (2022) 91–99.
- 879 [39] J. Wang, B. Yang, D. Li, C. Zeng, Y. Chen, Z. Guo, X. Zhang, T. Tan, H. Shu,
880 T. Yu, Photovoltaic cell parameter estimation based on improved equilib-
881 rium optimizer algorithm, *Energy Conversion and Management* 236 (2021)
882 114051.
- 883 [40] C. Xie, D. Wang, C. S. Lai, R. Wu, X. Wu, L. L. Lai, Optimal sizing of battery
884 energy storage system in smart microgrid considering virtual energy storage
885 system and high photovoltaic penetration, *Journal of Cleaner Production* 281
886 (2021) 125308.
- 887 [41] S. E. Ahmadi, N. Rezaei, H. Khayyam, Energy management system of net-
888 worked microgrids through optimal reliability-oriented day-ahead self-healing
889 scheduling, *Sustainable Energy, Grids and Networks* 23 (2020) 100387.
- 890 [42] X. Wen, D. Abbes, B. Francois, Stochastic optimization for security-constrained
891 day-ahead operational planning under pv production uncertainties: Reduc-

tion analysis of operating economic costs and carbon emissions, IEEE Access
9 (2021) 97039–97052.

[43] F. Meng, G. Dillingham, Life cycle analysis of natural gas-fired distributed combined heat and power versus centralized power plant, Energy & Fuels 32 (11) (2018) 11731–11741.

[44] visualcrossing, Weather query builder, <https://www.visualcrossing.com/weather/weather-data-services>.

[45] S. Peach, Carbon footprint of a wind turbine, <https://shorturl.at/cBEV7> (2021).

[46] HITACHI, Wind turbine, https://www.hitachi.com/products/energy/wind/products/htw2000_80/specification/index.html.

[47] Cool Effect, Carbon footprint of solar panel manufacturing, <https://www.cooleffect.org/solar-carbon-footprint>.

[48] European Commission, Photovoltaic geographical information system, https://re.jrc.ec.europa.eu/pvg_tools/en/tools.html#PVP.

[49] energy-stats.uk, User configurable dashboard, <https://shorturl.at/iACX5>.

[50] Nationalgrid ESO, Historical generation mix and carbon intensity, <https://data.nationalgrideso.com/data-groups/carbon-intensity1>.

[51] SunPower, Sunpower maxeon solar panels, https://sunpower.maxeon.com/uk/sites/default/files/2022-03/sp_max3_104c_com_380-400_dc_ds_en_a4_544454.pdf.

[52] Kia UK Limited, The soul ev, <https://www.kia.com/content/dam/kwcms/kme/uk/en/assets/vehicles/soul-ev/specification/kia-soul-ev-specification.pdf>.